Research Square

Preprints are preliminary reports that have not undergone peer review.
They should not be considered conclusive, used to inform clinical practice,
or referenced by the media as validated information.

Safety and Efficacy of a Mayaro Virus Vaccine Using an Insect-Specific Virus Platform

Scott Weaver

sweaver@utmb.edu

University of Texas Medical Branch at Galveston https://orcid.org/0000-0001-8016-8556

Jennifer Diaz

University of Texas Medical Branch at Galveston

Nisha Tapryal

The University of Texas Medical Branch at Galveston https://orcid.org/0000-0002-7598-4273

Mauricio Padilla

University of Texas Medical Branch at Galveston

Awadalkareem Adam

The University of Texas Medical Branch at Galveston

Xueyong Xu

Purdue University https://orcid.org/0009-0004-4087-3962

Andrei Siniavin

Gamaleya Center for Epidemiology and Microbiology https://orcid.org/0000-0001-7576-2059

Kristy Waldrep

University of Texas Medical Branch at Galveston

Kristyn Gonzales

University of Texas Medical Branch at Galveston https://orcid.org/0009-0002-7939-4139

Jesse Erasmus

HDT Bio Corp https://orcid.org/0000-0003-1612-2697

Farooq Nasar

University of Texas Medical Branch at Galveston

Ellie Hajovsky

University of Texas Medical Branch at Galveston

Jessica Plante

University of Texas Medical Branch https://orcid.org/0000-0002-4768-7458

Amanda Mareth

University of Texas Medical Branch at Galveston

Chanida Fonsaran

University of Texas Medical Branch at Galveston

Rachel Colwell

University of Texas Medical Branch at Galveston

Shilpa Sanapala

Washington University School of Medicine, St. Louis MO

Haiping Hao

University of Texas Medical Branch

Michael Diamond

Washington University in Saint Louis https://orcid.org/0000-0002-8791-3165

Richard Kuhn

Purdue University https://orcid.org/0000-0003-4148-1026

Tian Wang

University of Texas Medical Branch at Galveston https://orcid.org/0000-0002-1511-0793

Kenneth Plante

World Reference Center for Emerging Viruses and Arboviruses, University of Texas Medical Branch, Galveston, TX, USA https://orcid.org/0000-0002-7485-3167

Robert Abbott

University of Texas Medical Branch at Galveston https://orcid.org/0000-0003-0335-1175

Article

Keywords:

Posted Date: November 27th, 2026

DOI: https://doi.org/10.21203/rs.3.rs-11733124/v1

License: This work is licensed under a Creative Commons Attribution 4.0 International License. Read Full License

Additional Declarations: There is **NO** Competing Interest.

Abstract

Mayaro virus (MAYV) is an arthritogenic alphavirus endemic in parts of Central and South America, with the potential to cause urban epidemics. To develop a MAYV vaccine, we used the Eilat virus (EILV) platform, which utilizes chimeras of an insect-specific alphavirus that replicates only in mosquito cells. The structural proteins of EILV were replaced with those of MAYV to create a vaccine whose structural proteins are identical to MAYV but remained replication-defective in vertebrates. In C57BL/6J mice, EILV-MAYV induced robust humoral and cell-mediated responses, and the vaccine provided 100% protection against lethal MAYV challenge in A129 interferon receptor-defective mice. Dose-sparing studies showed females being better protected from death and viremia than males. Providing a booster dose, or increasing the priming dose ameliorated sex-based differences. In addition, one vaccination elicited durable neutralizing antibody responses and provided protection one-year post-vaccination. Overall, these data demonstrate the safety, immunogenicity, and efficacy of the EILV-MAYV vaccine.

Introduction

Mayaro virus (MAYV; species *Alphavirus mayaro*), an arthropod-borne alphavirus found in rural areas of Latin America, has the potential to emerge as an epidemic virus based on its ability to induce human viremia and to infect *Aedes aegypti* mosquitoes in laboratory experiments.[1] Additionally, the expanding geographic range of *Aedes aegypti* increases the risk of MAYV spread to northern latitudes, including in the United States.[2,3] In nature, MAYV is transmitted primarily in a sylvatic cycle between forest-dwelling *Haemagogus* mosquitos and nonhuman primates.[4] Humans living in rural areas near non-human primate populations can acquire spillover infections, with dozens-to-hundreds of cases reported each year. However, the true number of cases is unknown due to limited surveillance and MAYV infections' clinical appearance, which is similar to other infectious diseases, including dengue and chikungunya fever.[1] Infected humans can develop headache, fever, rash, swelling of the joints, joint pain, and muscle pain.[5,6] Up to 50% of cases can result in long-term arthralgia, which can be highly disabling, affecting the ability of patients to go about their activities of daily living.[7,8]

The combination of high viremia levels accompanying human MAYV infections and the vector competence of *A. aegypti* mosquitoes suggests the potential of MAYV to emerge in a pattern similar to chikungunya virus (CHIKV; species *Alphavirus chikungunya*), a closely related alphavirus that emerged from a sylvatic cycle in rural Africa.[1,4,5,9–11] CHIKV generates slightly higher viremia levels than MAYV,[12–14] and it more efficiently infects urban *A. aegypti* and *A. albopictus* mosquitoes,[15,16] allowing it to transmit within urban and suburban habitats.[11] MAYV is estimated to generate lower peak human viremia, and it infects roughly half of *A. aegypti* mosquitoes fed blood meals containing doses of 5.5 to 6.5 $\log_{10}$ plaque-forming units (PFU)/ml of MAYV.[17,18] Therefore, it may be possible for urban mosquitoes to become infected by feeding on MAYV-infected humans.[4] Small evolutionary adaptations to increase human viremia of MAYV or to more readily infect urban mosquito vectors, as occurred for

CHIKV in 2005,[15,19] could allow MAYV to emerge into urban cycles in South American cities, causing widespread illness and disability. It is therefore urgent to proactively develop vaccines against MAYV.

Because MAYV is prevalent in rural, resource-poor areas,[20] it is also essential to develop anti-MAYV vaccines that are cost-effective to manufacture and easy to distribute. This requires vaccines that are stable at 4°C rather than requiring ultra-cold temperatures. Additionally, a single-dose vaccine would be ideal, both to aid rapid deployment in the event of an epidemic and to facilitate durable protection of rural, hard-to-reach populations. Like all vaccines, anti-MAYV vaccines must be safe, with low potential for reactogenicity, reversion to virulence, or unintentional mosquito-borne transmission from vaccinees to others.

Eilat virus (EILV; species *Alphavirus eilat*) has been used as a platform to develop highly safe, stable, and affordable-to-manufacture alphavirus vaccine candidates.[21–24] EILV is an insect-specific alphavirus that was discovered in the Negev desert of Israel in a pool of *Anopheles coustani* mosquitoes.[25] Unlike typically pathogenic alphaviruses, EILV replicates only in mosquito cells, and it is restricted from replication in vertebrate cells at two stages.[25,26] The EILV structural proteins do not facilitate entry into vertebrate cells, presumably due to incompatible interactions with host-cell-surface receptor proteins.[26] In addition, bypassing viral attachment and entry by directly introducing EILV RNA into vertebrate cells via electroporation failed to initiate a productive replication cycle.[25] This is likely because the nonstructural proteins, in particular nsP3, fail to interact appropriately with vertebrate host cell proteins.[25,27] The latter host restriction makes EILV an ideal platform for the development of safe, chimeric alphavirus vaccines.

EILV-based chimeric vaccines are recombinantly generated by cloning the structural polyprotein open reading frame (ORF) of a pathogenic alphavirus into the EILV backbone containing the EILV untranslated genome regions and nonstructural polyprotein ORF.[21–24] These chimeric viruses retain the attachment and entry of pathogenic alphaviruses, enabling their entry into both mosquito and vertebrate cells to deliver the genomic RNA. However, the genomic RNA is unable to replicate because it contains the EILV nsP open reading frame (ORF), intergenic region, and 5' and 3' conserved sequence elements.[21,23] Therefore, EILV-based chimeras cannot replicate in human vaccine recipients, and thus cannot directly cause disease or be transmitted to mosquitoes. The EILV-based vaccines for CHIKV, Venezuelan equine encephalitis virus (VEEV), and eastern equine encephalitis virus (EEEV) have been shown to be safe and effective in animal models, including mice and non-human primates.[21–24] They induce long-lasting protection from disease, robust T-cell responses, and high neutralizing antibody titers in these models.[21,23,24,28]

Here, we describe the design and testing of an EILV-based vaccine to protect against MAYV infection. EILV-MAYV replicates to high titers in mosquito cell cultures, is genetically stable, and is safe in neonatal and immunocompromised mice. Additionally, a single vaccination with EILV-MAYV generates long-lasting T- and B-cell responses, as well as neutralizing antibodies, in a dose-dependent manner. The

vaccine therefore provides durable protection against lethal MAYV challenge in a type I interferon receptor-knockout ($IFNAR^{-/-}$) mouse model (A129).

Methods

All animal studies were carried out in accordance with the recommendations in the Guide for the Care and Use of Laboratory Animals of the National Institutes of Health and were approved by the Institutional Animal Care and Use Committee (IACUC) at the University of Texas Medical Branch (UTMB) (protocol 1708051B). A129 mice ($IFNAR^{-/-}$) were bred at UTMB Galveston. C57BL/6J mice (strain 000664) were purchased from Jackson Laboratories (Augusta, Maryland), and CD-1 mice (strain 022) were purchased from Charles River Laboratories (Wilmington, Massachusetts).

Cell culture

C7/10 *A. albopictus* cells were cultured in Dulbecco's Modified Eagle Medium (DMEM) (Gibco, Grand Island, New York, 11965092) + 10% (vol/vol) fetal bovine serum (FBS) (Gemini Bio, West Sacremento, California, S1150,) + 100 U/mL penicillin/streptomycin (Gibco) + 2% (vol/vol) tryptose phosphate broth (590 mg/L) (Sigma-Aldrich, St. Louis, Missouri, T8159-100 ml) + 1% (vol/vol) MEM non-essential amino acid solution 100x (Sigma-Aldrich, M7145) + 1 mM sodium pyruvate (Sigma-Aldrich, S8636) at 28ºC and 5% CO_2.. Cells were passaged by scraping and resuspending. Vero CCL-81 cells were cultured in Dulbecco's Modified Eagle Medium + 10% (vol/vol) FBS + 100 U/mL penicillin/streptomycin (Gibco) at 37ºC and 5% CO_2. Cells were passaged by washing in 1X DPBS (Gibco) and dissociating in 0.25% trypsin-EDTA (Gibco).

Generation of cDNA clones and rescue of infectious MAYV CH, EILV-MAYV, SINV-MAYV, and SINV-CHIKV clones

MAYV strain CH was rescued from an infectious cDNA clone[29] by linearizing the plasmid with the Pac1 restriction enzyme, purifying the DNA using phenol/chloroform extraction, and *in vitro*-transcribing using the mMessage machine Sp6 kit (Invitrogen, Carlsbad, California, AM1340) according to the manufacturer's protocol. Confluent Vero CCL-81 cells were trypsinized, washed three times in DPBS, and electroporated with the *in vitro* synthesized, capped RNA at 250 V, 3 pulses of 10 msec length each, 1 sec interval, in a 4 mm gap cuvette. After a 10-min incubation, the cells were mixed with DMEM + 10% (vol/vol) FBS + 100 U/mL penicillin/streptomycin and returned to the incubator at 37ºC and 5% CO_2. Virus was harvested at 2 days post-electroporation, when cytopathic effects became apparent. Cell debris was pelleted at 500 x g for 5 min, and the clarified supernatant was stored at -80ºC. This virus was used for challenge studies in adult mice.

To generate additional MAYV stocks for neutralizing antibody assays and for infant mouse neurovirulence studies, virus was passaged once on Vero CCL-81 cells at a multiplicity of infection (MOI)

of 0.1 in DMEM) + 10% (vol/vol) FBS + 100 U/mL penicillin/streptomycin.

The EILV-MAYV infectious clone was constructed using plasmid 7904, a modified EILV infectious clone derived from the previously described EILV-CHIKV construct.[30] In plasmid 7904, the viral structural protein genes had been removed and replaced with a unique XbaI restriction site. Plasmid 7904 was linearized with XbaI, and the MAYV structural gene cassette was PCR-amplified from the MAYV infectious clone p196.2 (p196.2 Mayaro ic cl2) using primers containing overlaps suitable for In-Fusion cloning. The amplified MAYV structural cassette and linearized plasmid 7904 backbone were assembled using an In-Fusion cloning reaction. Resulting clones were confirmed by sequencing and amplified in *E. coli* before plasmid preparation and subsequent *in vitro* RNA production.

Chimeric virus was then rescued from the infectious clone by linearizing with Not1-HF, purifying the DNA with phenol/chloroform extraction, and *in vitro* transcribing using the mMessage machine SP6 kit (Invitrogen) according to the manufacturer's protocol. Confluent C7/10 cells were scraped, washed three times in DPBS, and electroporated with the RNA for 5 pulses at 680 V for 99 us pulse length and a 200 msec interval, in a 4 mm gap cuvette. After a 10-min incubation, the cells were mixed with DMEM + 10% (vol/vol) FBS + 100 U/mL penicillin/streptomycin + 2% (vol/vol) tryptose phosphate broth (590 mg/L) + 1% (vol/vol) MEM non-essential amino acids 100X + 1 mM sodium pyruvate and returned to the incubator at 28ºC and 5% CO_2. Virus was harvested at 2 days post-electroporation, when cytopathic effects became apparent. Cell debris was pelleted at 500 x g for 5 min, and the clarified supernatant was stored at -80ºC.

To generate a replication-competent chimeric MAYV reporter virus expressing GFP, the structural polyprotein coding region from MAYV strain CH was incorporated into a cDNA backbone containing the Sindbis virus (SINV) nonstructural genes (nsP1-nsP4), with an eGFP reporter sequence inserted after the capsid gene in ORF2 (C-eGFP-E3-E2-6K-E1). The viral sequences were placed downstream of the SP6 bacteriophage promoter for *in vitro* RNA transcription. The resulting chimeric cDNA clone, designated pSINV-MAYV-CH-GFP, was synthesized and assembled into the plasmid vector by Twist Biosciences. Similarly, to create clone pSINV-CHIKV-LR-GFP, the structural polyprotein coding region of CHIKV strain LR was incorporated into the SINV cDNA backbone, an eGFP reporter sequence was inserted after the capsid gene, the viral sequences were placed downstream of the SP6 bacteriophage promoter, and the plasmid vector was sequenced by Twist Biosciences.

For virus rescue, 1 µg of plasmid DNA was linearized as a template for generating N^7-methylguanosine-capped genomic RNA using the HiScribe SP6 RNA Synthesis Kit, supplemented with 4 mM anti-Reverse cap analog (ARCA) (New England BioLabs, NEB, Ipswich, Massachusetts). Subsequently, 4 µg of in vitro transcribed RNA was electroporated into BHK-21 cells using a Gene Pulser Xcell electroporator with a 2 mm cuvette at 850 V and 25 µF. Supernatants were harvested as the P0 virus stock at 2 days after electroporation by pelleting the cell debris at 500 x g for 5 min. Higher-titer P1 stocks were generated by passage in Vero-furin cells[31] to promote efficient furin-dependent maturation of the viral glycoproteins. The P1 stock was quantified by focus-forming assay[32] on Vero-furin cells and used for subsequent

experiments. To confirm sequence integrity, RNA was extracted from the P1 stock supernatant using the MagMax Viral RNA isolation kit on a Kingfisher Flex instrument. cDNA was synthesized with random hexamers using ProtoScript II cDNA synthesis kit (NEB), the structural region was PCR-amplified, and the amplicon was purified with the ChargeSwitch PCR purification kit (Thermo Fisher Scientific) and subjected to Oxford Nanopore long-read sequencing (Plasmidsaurus, Louisville, Kentucky).

` For cryo-electron microscopy, concentrated stocks of EILV-MAYV were produced by passaging the recovered infectious clone-derived virus once in C7/10 cells. Flasks containing 90–100% confluent C7/10 cells were infected at a MOI of 0.1 PFU/cell. Cells were monitored until approximately 50% cytopathic effect (CPE) was observed, approximately 2 days post-infection. The supernatants were harvested and clarified by centrifugation at 500 × g for 5 min at 4°C. The clarified supernatants were then concentrated by ultracentrifugation at 175,000 × g (32,000 rpm) using an SW41 Ti rotor over a 24% (w/v) sucrose cushion prepared in sterile TNE buffer (50 mM Tris-HCl (Invitrogen), pH 7.4, 0.12 M NaCl (Invitrogen), and 1 mM EDTA (Invitrogen). The resulting pellets were resuspended in sterile 1× TNE buffer. The concentrated virus was aliquoted and stored at − 80°C. For further purification, the virus pellet was resuspended and purified by ultracentrifugation through a 30–60% OptiPrep gradient (Sigma) at 32,000 rpm for 2 h. Buffer exchange was performed using an Amicon Ultra-4 centrifugal filter with a 100-kDa molecular-weight cutoff (MilliporeSigma, Z648043-24EA) into 1× TNE.

Virus titration

To titrate EILV-MAYV, C7/10 cells were plated the previous day at $1x10^6$ cells/well in a 6 well plate. Virus was serially diluted in DMEM + 10% (vol/vol) FBS + 100 U/mL penicillin/streptomycin + 2% (vol/vol) tryptose phosphate broth (590 mg/L) + 1% (vol/vol) MEM non-essential amino acids 100X + 1 mM sodium pyruvate. Medium was gently removed from each well of cells, and 0.5 mL of medium was replaced onto each well. 100 ul of each virus dilution were plated on a well. Cells were infected for 1 h, rocking every 10 min. Then, 3 mL/well of overlay (1 part 2% sterile tragacanth in water, 1 part 2×MEM with 10% FBS, 200 U/mL penicillin/streptomycin was added gently to each well. After 3 days, cells were fixed in 10% neutral buffered formalin (Epredia, 5701) for 24 h and were stained with 0.25% crystal violet.

MAYV strain CH was titrated as previously described.[33] Briefly, Vero CCL-81 cells were plated to 90–100% confluent on the day of titration. Virus was serially diluted in DMEM + 2% FBS + 100 U/mL penicillin/streptomycin. Medium was removed from each plate, and 250 uL of each dilution was plated on each well of the plate. Cells were infected for 1 h, then 4 mL/well of 0.8% agarose overlay was added. Cells were fixed in 10% neutral buffered formalin at 2 days post-infection and stained with 0.25% crystal violet.

Cryo-EM grid preparation, data collection and image processing

A 3-µL aliquot of purified EILV-MAYV particles was applied to glow-discharged lacey carbon grids with a continuous ultrathin carbon-film support (Ted Pella, Redding, CA, 01824). The grids were incubated in a humidity-controlled chamber at 12°C and 100% relative humidity for 1 min, blotted for 8–14 s using filter paper (Whatman, Florham Park, New Jersey, USA, 1001-070), and plunge-frozen in liquid ethane using a Leica EM GP2 inside a BSL-2 biosafety cabinet. Cryo-EM datasets were acquired on a Thermo Fisher Titan Krios G4 microscope operated at 300 kV and equipped with a Gatan K3 direct electron detector operated in counting mode and a post-column Gatan Quantum GIF energy filter with a 20-eV slit width. A total of 4,864 movie stacks was collected at defocus values ranging from − 0.6 to − 2.0 µm. Each movie stack was recorded with a total exposure dose of 57.36 $e^{-}/Å^2$ over 3.21 s and was fractionated into 50 frames. Movies were acquired automatically using EPU software at a nominal magnification of 81,000×, corresponding to a pixel size of 1.058 Å. Image processing was performed using the CryoSPARC software platform[4]. Movie stacks were pre-processed using Patch Motion Correction and Patch CTF Estimation. Particles were selected using a template picker and subsequently subjected to two- and three-dimensional classification. A whole virus reconstruction was generated using homogeneous and non-uniform refinement with icosahedral symmetry imposed. To obtain a high-resolution reconstruction of a single asymmetric unit, particles were symmetry-expanded using icosahedral symmetry, followed by subparticle extraction and local refinement. The sub-volume corresponding to a single asymmetric unit was selected to generate the corresponding masks. The resulting masked local reconstruction of the asymmetric unit reached a nominal resolution of 2.51 Å (**Supplementary Table S1**).

The atomic model was built based on the 2.51Å local reconstruction. The cryo-EM structure of MAYV[34] was used as the starting model and rigid-body fitted into the density map using ChimeraX[5]. The model was subsequently manually adjusted in Coot[6] and refined using phenix.real_space_refine[7] (**Supplementary Table S1**).

Serial passaging and RNA sequencing

C7/10 cells were plated to be 90–100% confluent on the day of infection. EILV-MAYV was used to infect cells at a MOI of 0.01. Supernatants were harvested when at least 50% of cells displayed cytopathic effects. Subsequent passages were performed blindly by diluting supernatants from the previous passage 1:10 and using 20 µL of this dilute working stock to infect a T25 flask. After each passage, supernatants were stored at -80ºC, then mixed 200 µL with 1000 µL of Trizol-LS reagent (Invitrogen, 10296010), and RNA was isolated according to the manufacturer's instructions.

RNA sequencing libraries were prepared using New England BioLabs NEBNext Ultra II RNA Library Preparation kit either with or without ribosomal RNA depletion following the manufacturer's recommended procedures. The finished libraries were quality checked on Agilent Bioanalyzer 2100 and quantified using real time PCR. The libraries were pooled and sequenced on Illumina NextSeq 550 or Element Biosciences' AVITI for paired end 75 bp reads, targeting 5–25 million read pairs per sample.

The raw sequencing reads were filtered by removing low quality reads and bases and any adapter sequences using Trimmomatic (v.0.39) software program[35]. The trimmed and filtered reads were assembled into long *de novo* contigs using ABySS v.2.3.4 and contigs are clustered using CD-HiT v.4.8.1. The resulting contigs longer than 400 bases were searched against the GenBank database and a custom viral protein sequence database using the NCBI BLAST program (v.2.11.0). The contigs ends were fixed using kmer and jellyfish (v.2.3.0) and manually inspected and joined when overlapping. The filtered reads of each sample were then mapped to the near full-length viral genome obtained and LoFreq (v.2.1.5) variant caller was used to call variant bases.

EILV-MAYV vaccine production and purification

For studies in adult mice, concentrated stocks of EILV-MAYV were generated by passaging the virus once on C7/10 cells. Flasks of 90–100% confluent C7/10 cells were infected at a MOI of 0.1. When cells reached approximately 50% cytopathic effects (CPE), at approximately two days post-infection, supernatants were harvested and clarified by centrifuging at 500 x g for 5 min at 4ºC. Clarified supernatants were then mixed 3:1 with 4x polyethylene glycol (PEG) (28% polyethylene glycol (Sigma-Aldrich), 9.2% NaCl, in molecular grade water, autoclaved). The supernatant/PEG mixture was allowed to precipitate overnight at 4ºC, and then centrifuged at 3100 x g at 4ºC for 30 min. The supernatant was removed from the pellet, the pellet was washed gently with ice-cold sterile 1X TEN buffer (0.05M Tris-HCL, 0.1M NaCl, 0.001 M EDTA), and resuspended in sterile 1X TEN buffer. The vaccine was aliquoted and stored at -80ºC.

To generate highly concentrated stocks of EILV-MAYV for neurovirulence studies in infant mice, EILV-MAYV was passaged as described above. The supernatant was then concentrated using an Amicon Ultra-4 100kDa molecular weight cutoff centrifugal filter, and the virus was resuspended in sterile 1X DPBS.

Mouse neurovirulence studies

Pregnant CD-1 female mice were obtained from Charles River Laboratories, and their one- to three-day-old pups were used for neurovirulence studies. Animals were anesthetized with isoflurane, then injected intracranially with 20 µL of DPBS, 10^8 PFU of EILV-MAYV in DPBS, or 10^4 PFU of MAYV in DPBS. For ten days, animals were weighed and observed daily for signs of disease, and euthanized upon any loss of weight or failure to gain weight in any 24 h period.

To assess the ability of EILV-MAYV to replicate upon serial passage, intracranially infected animals were euthanized at 2 days post-infection, brains were pooled and homogenized in nine volumes by weight of sterile 1X DPBS and frozen at -80. The homogenate was then clarified by centrifugation at 500 x g for 5 min, filter-sterilized through a 22 µm syringe filter, and used to infect the subsequent litter at 20 uL/animal. Homogenates were titrated by plaque assay as described above.

Mouse immunogenicity studies

Six-to-7-week-old C57BL/6J mice were purchased from Jackson Laboratory. Age- and sex-matched male and female mice were vaccinated intraperitoneally (i.p) with 10^8 PFU of EILV/MAYV or PBS (mock). At 30 or 60 days post-vaccination, mice were euthanized. Spleen and blood samples were collection for T-cell and antibody responses analysis.

Mouse vaccine challenge studies

Six-to-8-week-old IFNAR$^{-/-}$ A129 mice were vaccinated with the indicated doses subcutaneously (s.c.) in 200 µL of PBS. Mice were bled retro-orbitally at the indicated time points, serum was assayed for neutralizing antibody assay using the focus reduction neutralization test $(FRNT)_{80}$ described below, and serum viremia was measured by plaque assay as described above. Following the indicated incubation times, animals were challenged with the indicated doses of MAYV strain CH, monitored daily for weight loss and disease, and their footpads were measured using a digital caliper under isoflurane anesthesia at the indicated time points. Animals were euthanized at the onset of severe disease (> 20% weight loss, neurologic disease, lethargy). Survival proportions were analyzed in Prism 10.6.1 (GraphPad Software, Inc.) using a Kaplan-Meier test.

Mouse B-cell studies

Female C57BL/6J mice were purchased from the Jackson labs. EILV-MAYV immunizations were prepared by diluting EILV-MAYV in PBS for a dose of 10^7 PFU per mouse ($5*10^7$ PFU/mL), then administered subcutaneously (s.c.) at the tail base in a bilateral fashion (total volume 200 µl, 100 µl per side). On the day of harvest, the draining lymph nodes (inguinal and popliteal) from both sides of the mouse were collected. All mice were housed under specific pathogen-free conditions at UTMB. All mouse experiments were done under approved Institutional Animal Care and Use Committee protocols at UTMB.

Plaque-reduction neutralizing antibody tests

PRNTs were performed using MAYV strain CH and Vero cells (ATCC CRL-1587). Briefly, serum samples were heat-inactivated at 56°C for 30 min and serially diluted two-fold in infection medium (MEM supplemented with 2% heat-inactivated FBS and 1× antibiotic-antimycotic). Diluted sera were mixed 1:1 with MAYV at 800 PFU/mL, resulting in approximately 40 PFU per 100 µL of inoculum, and incubated overnight at 4°C. The serum–virus mixtures were then inoculated onto confluent Vero cell monolayers in 12-well plates and incubated at 37°C for 1 h. Following adsorption, cells were overlaid with infection medium containing 0.4% agarose and incubated at 37°C for 60 h. Plates were fixed with 10% formaldehyde, stained with 0.25% crystal violet in 30% methanol, and plaques were counted. $PRNT_{50}$ titers were calculated using GraphPad Prism and defined as the reciprocal serum dilution resulting in a 50% reduction in plaque numbers compared with control wells containing no serum.

Focus-reduction neutralizing antibody assays

Vero CCL-81 cells were plated the day prior to titration at 3.1 x10^4 cells/well in a 96-well plate. The day of titration, antibodies were serially diluted 1:2 in 1X DPBS + 2% (vol/vol) FBS + 100 U/mL penicillin/streptomycin. MAYV was diluted to 4000 FFU/mL, and it was mixed 1:1 with the serum dilutions. The serum with virus was incubated for 1 h at 37ºC and 5% CO_2. Twenty µL of serum with virus was plated on each well, the cells were infected for 1 h at 37ºC and 5% CO_2, and 150 µL of overlay (Opti-MEM (Gibco) with 1% w/v carboxymethylcellulose (Sigma) + 2% FBS + 100 U/mL penicillin/streptomycin was added gently to each well. Plates were fixed 20–22 h post-infection in 10% neutral buffered formalin.

Plates were immunostained by blocking overnight in 5% (w/v) nonfat powdered milk (Genessee Scientific, Apex 20–24) in PBS by incubating for 1 h with mouse anti-MAYV mouse immune ascitic fluid (from the World Reference Center for Emerging Viruses and Arboviruses at UTMB) at a 1:2000 dilution in 5% w/v nonfat powdered milk in PBS, washing three times in PBS, incubating 1 h in HRP-linked goat anti-mouse IgG (SeraCare, 5450-0011)) at a 1:2000 dilution in 5% w/v nonfat powdered milk in PBS, washing three times in PBS, and incubating with KPL TrueBlue Peroxidase Substrate (SeraCare) until blue foci appeared. Plates were imaged on the BioTek Cytation 5 (Agilent).

The 80% plaque neutralization titers ($FRNT_{80}$) were calculated by non-linear regression analysis using Prism 10.6.1 after determining the percent of plaques at each dilution relative to control wells containing no serum.

Neutralization assays using SINV-MAYV and SINV-CHIKV

GFP-based FRNTs were performed using the chimeric SINV-MAYV-CH-GFP or SINV-CHIKV-LR-GFP and Vero-furin cells. Cells were seeded the night before the assay at 2.5 x 10^4 per well into 96-well plates in DMEM supplemented with 10% (v/v) FBS (Omega Scientific), 10 mM HEPES pH 7.3 (Gibco), 1% non-essential amino acids, 1% GlutaMax (Gibco), and 1% penicillin/streptomycin. Serum from EILV-MAYV-immunized mice was heat-inactivated at 56°C for 30 min and then serially diluted (three-fold beginning at 1/50) immediately prior to incubation with ~ 200 FFU of SINV-MAYV-CH-GFP for 1 h at 37ºC and 5% CO_2. The serum-virus mixture was then added to Vero-furin cells and incubated for 1 h at 37ºC and 5% CO_2 followed by the addition of 1% (w/v) methylcellulose overlay in MEM. Cells were fixed at 20 h post-inoculation with 4% paraformaldehyde (Electron Microscopy Sciences) in PBS for 10 min. Infected cell foci were visualized under a FITC channel (using an excitation band of 480 nm, gain setting of 28.0, exposure setting of 2800 ms, and zoom setting of 1.8x) and quantitated on an ImmunoSpot microanalyzer (Cellular Technologies). The effective concentration of 50% inhibition (EC_{50}) values was interpolated using a 4-parameter nonlinear regression in GraphPad Prism 10.6.1. Positive controls, including mAbs MAY-118 [36] and 506.C0[37]1 for MAYV, and CHK-152[38] and 506.CO1 for CHIKV, as well as two positive immune serum with known EC_{50} values, were run in parallel for each assay.

IFN-γ ELISPOT

ELISPOT plates (Millipore Ltd, Burlington, MA) were coated with mouse anti-IFN-γ capture Ab at 1:100 dilution (Cellular Technology Ltd, mIFNg-1M/10) and incubated at 4°C overnight. Splenocytes were stimulated with MAYV E1, E2, E3 recombinant proteins (Alpha Diagnostic Intl. Inc, MAYV11-R-100, MAYV12-R-100, MAYV61-R-100), virus-like particles (C-E3-E2-6K-E1, VLP; Native Antigen, REC31616), or CHIKV E2 recombinant protein (Sino Biological, Inc) (1 µg/mL, Miltenyi Biotec, 40440-V08B) for 24 h at 37°C. Cells stimulated with anti-CD3 (1 µg/mL, e-Biosciences, 14-0032-82) or medium alone were used as controls. This was followed by incubation with biotin-conjugated anti-IFN-γ at 1:100 dilution (Cellular Technology Ltd, mIFNg-1M/10) for 2 h at room temperature, followed by incubation with alkaline phosphatase-conjugated streptavidin for 30 min. The plates were washed and scanned using an ImmunoSpot 6.0 analyzer and analyzed by ImmunoSpot software (Cellular Technology Ltd) to determine the spot-forming cells (SFC) per 10^6 splenocytes.

MAYV IgG ELISA

ELISA plates were coated with 100 ng/well of recombinant MAYV E2 protein (Alpha Diagnostic Intl. Incl) overnight at 4°C. The plates were washed twice with PBS, containing 0.1% Tween-20 (PBS-T) and then blocked with 2% BSA for 2 h at room temperature (RT). Sera were serial diluted in blocking buffer and 100 µL were added per well for 1 h at RT. Plates were washed five times with PBS-T. Anti-mouse IgG (Sigma) coupled to alkaline phosphatase (AP) was added as the secondary antibody at a 1:1000 dilution for 1 h at RT. Color was developed with AP substrate and the intensity was read at an absorbance of 405 nm. Binding endpoint titers were determined using a cutoff value which is negative control+3x SD.

Histology

Inguinal lymph nodes were frozen in Tissue-Tek (Electron Microscopy Sciences) in a liquid nitrogen-cooled bath of 2-methylbutane. 6 µm-thick cryosections were cut from each lymph node in a cryostat set to -18°C. Sections were then adhered to Colorfrost Plus™ slides (Fisherbrand), air-dried for 2 hours at RT, and fixed in a 1:1 mixture of acetone and methanol for 10 minutes at -30°C. Sections were allowed to air-dry, then were covered with Epredia Shandon plastic coverplates (Fisher Scientific) and washed with of PBS + 0.5% BSA + 0.1% Tween-20 (wash/stain buffer) in a Freequenza rack box (UTMB 3D Printing Core) for 10 min to rehydrate. Sections were treated with Fc block (clone 2.4G2, BD Biosciences) at a 1:50 dilution and incubated at room temperature for 30 min, then stained with the following mAbs at 1:200 dilutions each at room temperature for 1 h: [B220-(BV421) clone RA3-6B2, GL7-(PE), TCRβ-(A488) clone H57-597] (BioLegend). Sections were then washed 3 times with wash/stain buffer and mounted with a 1.5 number coverslip using ~ 35 uL of Fluoromount G (SouthernBiotech). Sections were imaged with a Zeiss Axio Scan.Z1 slide scanner equipped with Zen acquisition software, then processed with QuPath version 0.4.4.[39]

Flow Cytometry

Collected bilateral draining lymph nodes were pooled (2 inguinal and popliteal lymph nodes per mouse) and mechanically dissociated to create single-cell suspensions in FACS buffer (5% FCS/PBS). Cells were then counted, Fc-blocked (clone 2.4G2, BD Biosciences) for 10 min at 4°C and stained for 30 min at 4°C

with a mix of mAbs (BioLegend and BD Biosciences) and streptavidin-conjugated MAYV p62-E1^{40} baits. Cells were then washed and fixed in a Foxp3 fixation kit solution (eBioscience) and, if appropriate, stained with secondary intracellular mAbs the next day. Samples were acquired on a NovoCyte Penteon (Agilent) and analyzed on FlowJo v10.10.0. The following anti-mouse antibody clones were used for staining: 11-26c.a2 (IgD), II/41 (IgM), GL-1 (CD86), 281-2 (CD138), RMG-1 (IgG1), RA3-6B2 (B220), GK1.5 (CD4), GL7 (GL7), L276F12 (CXCR4), 90 (CD38), LI38D7 (CXCR5), 53 – 2.1 (CD90.2), 29F.1A12 (PD-1), IM7 (CD44), C398.4A (ICOS), UC10-4B9 (CTLA-4), MF-14 (FoxP3), and 8F10 (TACI). MAYV p62-E1 flow baits were prepped by biotinylating Avi-tagged MAYV p62-E1^{40} using a BirA kit (Avidity). Single-color streptavidin (SA) conjugated MAYV p62-E1 baits were then prepared by mixing biotinylated MAYV p62-E1 with the following individual streptavidin fluorophores (BioLegend) at room temperature in the dark for 30 minutes: SA-APC (cat# 405243), SA-PE (cat# 405204), SA-BV421 (cat# 405225).

Results

Production and characterization of EILV-MAYV

To create an anti-MAYV vaccine, we cloned the structural polyprotein ORF of MAYV into the EILV backbone to create the EILV-MAYV infectious cDNA clone (Fig. 1A). We rescued virus from the clone in C7/10 cells, then passaged it once to generate high titer virus stocks, with EILV-MAYV replicating to over 10^8 PFU/ml.

To characterize the morphological features of EILV-MAYV, we performed cryo-electron microscopy (Fig. 1B-E). The EILV-MAYV structure was determined at a global resolution of 3.1Å (**Fig. S1A**). Density corresponding to the E3 protein was not observed, consistent with the structure of mature MAYV particles[1]. EILV-MAYV exhibits the characteristic structural organization shared by mature particles of other members of the Alphavirus genus. The 80 spikes, each composed of a trimer of E1–E2 heterodimers, assemble into particles approximately 700Å in diameter with *T = 4* icosahedral symmetry. Superposition of the EILV-MAYV and MAYV cryo-EM maps yielded a cross-correlation coefficient of 0.6647, indicating good overall structural agreement between the two particles (Fig. 1B).

Local resolution estimation of the EILV-MAYV density map showed that the capsid and membrane-proximal regions of E1 and E2 were resolved at relatively high resolution, whereas the membrane-distal region of E2 exhibited substantially lower resolution, consistent with its greater conformational flexibility (**Fig. S1B**). A similar variation in local resolution was observed in the structure of mature MAYV. To improve the resolution of the EILV-MAYV asymmetric unit and resolve additional structural features, we performed symmetry expansion followed by subparticle extraction and local refinement of individual asymmetric units. This procedure yielded a 2.51Å resolution map (**Fig. S1C-D**), enabling accurate modelling of distinct side-chain conformations and glycans at the glycosylation sites (**Fig. S1E** and Fig. 1C). Furthermore, the high-quality density corresponding to the transmembrane domains of E1 and

E2 enabled unambiguous model building, which was not possible in our 3.1Å whole-virus reconstruction or in the previously reported lower-resolution structures of MAYV (**Fig. S1F**).[34,41]

Two glycosylation sites have been identified in MAYV: N141 in E1 and N262 in E2. The N141 glycosylation site in the E1 envelope protein is important for alphavirus infection of host cells, whereas the N262 glycosylation site in E2 forms a stable carbohydrate "handshake" that connects adjacent viral spikes, thereby stabilizing the particle structure and potentially modulating binding to the mammalian receptor MXRA8.[42] Both glycosylation sites were clearly resolved in the EILV-MAYV density map (Fig. 1C). Two N-acetylglucosamine (NAG) residues could be unambiguously modelled at the N262 glycosylation site, whereas only one NAG residue could be modelled at N141. The absence of density for the remaining portions of the glycans suggests that these carbohydrate chains are highly flexible, consistent with observations from cryo-EM structures of MAYV and EEEV.[34,43]

In the MAYV density map, a cavity between E1 and E2 at the outer leaflet of the membrane is occupied by continuous additional density that can be fitted with a C18 hydrocarbon chain.[34] A similar density was clearly identifiable in the EILV-MAYV density map (Fig. 1D). As observed in MAYV, the aromatic group of Y358 in EILV-MAYV forms close hydrophobic contacts with this molecule, while polar residues, including H362, T365, and T366, also contact the molecule (Fig. 1E). These interactions suggest that the molecule has amphipathic properties and may correspond to a fatty acid.

In summary, EILV-MAYV particles closely resemble mature MAYV particles in their overall icosahedral organization, as well as in the positions of the two glycosylation sites and the amphipathic molecule within the cavity between E1 and E2, confirming the antigenic authenticity desired in the chimeric vaccine.

Genetic stability of EILV-MAYV in C7/10 cells

EILV-MAYV is produced by passaging in C7/10 cells, so its genetic stability was tested by passage in this cell line. Deep sequencing of passages 0, 1, 5, and 10 revealed that only one mutation (Gly to Glu in E2-186) arose to levels > 10% in multiple replicates. By passage 5, the mutation was detected at 0% 19%, and 22% prevalence in the three parallel passage series (**Fig. S2**). This low mutation rate by passage 5 is notable because the manufacture of large seed stocks for vaccine production is expected to requires up to 5 passages.[44] To examine whether the observed mutations would increase in frequency, we continued for ten total passages, by which point we observed 0%, 46%, and 77% prevalence of E2 G186E (**Fig S2, Supplementary Table S2**). Even by passage 10, no consensus mutations arose in the nonstructural proteins, which are responsible for the inability of the vaccine to replicate in vertebrates.[26]

Safety and efficacy of EILV-MAYV in mice

The replication capacity of EILV-MAYV was investigated in infant CD-1 mice via intracranial injection at 10^8 PFU/mouse (Fig. 2A-B).[45,46] Similar to sham treated mice, all infected mice exhibited no overt disease, gained weight, and survived. (Fig. 2A-B). In contrast, mice injected with a lower 10^4 PFU/mouse

dose of wild-type (wt) MAYV displayed weight loss within two days, requiring euthanasia. Serial passage of EILV-MAYV in infant mice via i.c. route did not produce detectable replication; the low infectious titer in the passage 1 brains were presumably residual carry-over from the high titer inoculum used to initiate the passages (Fig. 2C).

The efficacy of EILV-MAYV vaccine was investigated in the A129 mouse model. The A129 mice lack type I IFN receptor, thus rendering it highly susceptible to lethal virus infections. Six-to-eight-week-old A129 mice were vaccinated subcutaneously with 10^8 PFU of EILV-MAYV. Niether vaccinated nor sham-treated mice exhibited disease signs or weight loss following vaccination (Fig. 2D). One month following a single vaccination, mice were challenged with a lethal dose of wt MAYV strain CH (10^5 PFU) in the footpad. Disease signs, footpad swelling, and weight were assessed daily, and viremia was measured on day two post-challenge. All sham-vaccinated mice succumbed to challenge by day three, whereas vaccinated mice were completely protected from death, weight loss, and disease signs (Fig. 2E-G). Both vaccinated and sham treated mice developed ipsilateral footpad swelling (Fig. 2G). Lastly, unvaccinated mice developed viremia exceeding 10^8 PFU/mL, whereas vaccinated mice were fully protected, with no detectable viremia (Fig. 2H).

Efficacy of EILV-MAYV against heterologous challenge

Next, the efficacy of EILV-MAYV in protecting of EILV-MAYV against heterologous arthritogenic alphaviruses was assessed. Initially, to examine antibody responses in an immune-intact animal model, C57BL/6J mice were vaccinated with either EILV-MAYV or EILV-CHIKV,[21,22] and antibodies binding to the heterologous virus E2 protein were measured by ELISA. EILV-MAYV induced detectable antibody response against MAYV E2 and CHIKV E2 (**Fig. S3A-B**). Therefore, we proceeded to assess the efficacy of EILV-MAYV protection against lethal CHIKV and Ross River virus (RRV; species *Alphavirus rossriver*, another related alphavirus in the Semliki Forest complex) challenge. Six-to-eight-week old A129 mice were vaccinated as described above and challenged with 10^4 PFU of MAYV, RRV, or CHIKV at 28 days post-vaccination (**Fig. S3C-F**). At one-month post-vaccination, A129 mice displayed detectable neutralizing antibodies against MAYV using a high-throughput fluorescence-based neutralization assay, with females displaying a mean IC_{50} of 366, and males, 97 (**Fig. S3C**). Neutralizing antibodies against CHIKV, however, were not detected, with a limit of detection of IC_{50}= 100 (**Fig. S3D**). Similar to studies above, EILV-MAYV-vaccinated mice challenged with lethal MAYV were protected from death, weight loss, and viremia. In contrast, all mice challenged with CHIKV or RRV succumbed to infection by day three or day two, respectively (**Fig. S3E-F)**. EILV-MAYV-vaccinated mice developed similar RRV viremia to sham-vaccinated mice, indicating no protection (**Fig. S3G**). Nonetheless, EILV-MAYV-vaccinated mice displayed slightly reduced CHIKV viremia at day two post-challenge compared to unvaccinated mice, indicating a low level of cross-protection (**Fig. S3G**). Protection from footpad swelling was not observed for any vaccine-challenge virus combination (**Fig. S3H**). In summary, EILV-MAYV protected robustly against MAYV but exhibited little or no cross-protection against other clinically significant arthritogenic alphaviruses in highly immunodeficient A129 mice.

EILV-MAYV dose-dependently protects against MAYV challenge.

Next, the optimal dose of EILV-MAYV was assessed in the A129 mouse model. Six-to-eight-week-old mice (three male and three female per group) were vaccinated with 10^8, 10^7, or 10^6 PFU/mouse of EILV-MAYV, then challenged at day 28 post-vaccination. Mice did not lose weight following vaccination with any dose, indicating that the vaccine was well tolerated (Fig. 3A). However, upon lethal challenge with MAYV strain CH, 50% of mice vaccinated with 10^6 PFU/mouse and 33% of mice vaccinated with 10^7 PFU /mouse succumbed to infection on day three post-challenge (Fig. 3B-C). Additionally, at day two post-challenge, 100% of mice vaccinated with 10^6 PFU/mouse and 50% of mice vaccinated with 10^7 PFU/mouse had detectable viremia, but those vaccinated with 10^8 PFU/mouse were fully protected from death and viremia (Fig. 3B, D). Of note, with the 10^6 PFU dose, all challenged mice developed signs of disease (ruffled fur, hunched posture), but only males succumbed to disease. With the 10^7 PFU dose, a single male and a single female succumbed, and no other mice developed disease signs. Only the 10^8 PFU dose elicited detectable neutralizing antibodies by 14 days post-vaccination, and it induced the highest titers of neutralizing antibodies at 28 days post-vaccination (Fig. 3E). However, no dose conferred protection from footpad swelling (Fig. 3F**)**; 10^8 PFU of EILV-MAYV was therefore determined to be the optimal single dose in this model system.

Booster doses improve protection by EILV-MAYV

We next tested whether the administration of a booster could increase the efficacy of the 10^7 PFU dose of EILV-MAYV (Fig. 4). We vaccinated adult A129 mice (five male and five female per group) with 10^7 PFU or 10^8 PFU of EILV-MAYV. After one month, we sham-boosted with PBS or boosted with a second, equivalent dose of EILV-MAYV. At one-month post-boost (2-months post-prime vaccination), we challenged with a lethal dose of MAYV. In both sexes, all PBS-vaccinated mice lost weight, developed high viremia, and succumbed to infection by day three post-challenge (Fig. 4A-E). Mice that received a single vaccination of 10^7 PFU followed by a sham booster demonstrated the greatest footpad swelling after challenge (Fig. 4F). Females in this group did not lose significant weight, all developed only low-level viremia (< 4.5 $\log_{10}$ PFU/ml), and one succumbed to infection. In contrast, males receiving a single 10^7 PFU dose followed by a sham booster lost significant weight, 100% developed viremia (3.8–7.4 $\log_{10}$ PFU/ml), and 80% succumbed to infection.

Administration of a second EILV-MAYV dose of 10^7 PFU improved protection for both sexes. Females were 100% protected from death and viremia (Fig. 4A, E), whereas males were 80% protected from death (Fig. 4B**)**, and 60% of males developed low but detectable viremia (≤ 4 $\log_{10}$ PFU/ml), (Fig. 4E). Either one or two doses of 10^8 PFU of EILV-MAYV fully protected both sexes from death and from disease signs other than footpad swelling. However, one male mouse that received a single dose of 10^8 PFU EILV-MAYV developed a very low level of viremia at day two (2.7 $\log_{10}$ PFU/ml) (Fig. 4E). Additionally, mice receiving two 10^8 PFU doses of EILV-MAYV demonstrated significantly reduced footpad swelling

compared to sham-vaccination with PBS, whereas those receiving one dose were not protected (Fig. 4F). Thus, administration of a booster increased protection from MAYV disease in the A129 mouse model. However, even two doses of 10^7 PFU remained inferior to a single dose of 10^8 PFU. Similarly, male and female mice had the greatest neutralizing antibody responses to two doses of either 10^7 PFU or 10^8 PFU, with inferior responses at a single dose of 10^7 PFU (Fig. 4G). Interestingly, with one dose of 10^8 PFU, female mice had a lower response than males at two-months post-prime despite their higher response at one-month post-prime, indicating that the male neutralizing antibody response at this dose continued to increase, but the females did not.

T cells and sex differences in correlates of protection elicited by EILV-MAYV

To assess the immunogenicity of EILV-MAYV in immunocompetent animals, 6-week-old female C57BL/6J mice were vaccinated i.p. with 10^8 PFU, and antibody levels were assessed at 1- and 2-months post-immunization. High levels of anti-MAYV E2 binding antibodies were detected by ELISA (mean values of 23,040 and 46,080 at 1- and 2-months post-vaccination, respectively) (Fig. 5A) and neutralizing antibody were detected by PRNT (mean $PRNT_{50}$ of 1:6,880 and 1:12,170 at 1- and 2-months, respectively) (Fig. 5B). Additionally, vaccine-specific T cell responses were assessed at 1- and 2-months post-vaccination by isolating splenocytes, stimulating them with MAYV E1, E2, and E3 proteins, VLPs, or CHIKV E2, and measuring the number of cells producing IFN-γ by ELISpot assay (Fig. 5C, D). At 1- and 2-months post-vaccination, over 200 and 100 MAYV E1-specific cells per 10^6 total splenocytes were detected, respectively. T cells specific to other MAYV epitopes and to CHIKV-E2 were detected at lower frequencies at both time points.

Because we observed differences in the efficacy of EILV-MAYV between male and female mice, we assessed sex differences in immune responses at one-month post-vaccination. While females and males displayed similar total anti-MAYV IgG levels, females had higher anti-MAYV E1 T cell responses (Fig. 5E-G). The more robust T cell and neutralizing antibody responses detected in female mice correlated with the improved protection conferred by EILV-MAYV against lethal challenge of females (Fig. 4).

EILV-MAYV elicits a germinal center B cell response

Given the strong protection and neutralizing antibody titers induced by EILV-MAYV (Fig. 2–4), we further investigated the ability of this vaccine to induce antigen specific B cell responses. Following vaccination, antigen-activated B cells proliferate and enter germinal centers (GCs). GCs are the anatomic site in which antigen-activated B cells undergo somatic hypermutation of their antibody encoding genes.[47] Over the weeks and months following vaccination, GC B cells undergo rounds of mutation followed by T follicular helper cell (Tfh) mediated selection to generate high affinity protective antibody responses.[48]

To assess the induction of GCs in response to EILV-MAYV, we immunized immunocompetent C57BL6/J mice subcutaneously and evaluated the immune response in draining lymph nodes 12 days post-

immunization. EILV-MAYV-immunized mice showed an increased frequency of GCs compared to naïve mice **(**Fig. 6A-B, **Fig S4A)**. To evaluate the antigen specificity of the GC response, we stained GC B cells with avi-tagged MAYV p62-E1 baits. MAYV p62-E1 is a viral precursor protein expressed on the surface of the virion and contains multiple epitopes important for neutralization.[40] EILV-MAYV not only induced a significant GC B cell response, but also a substantial fraction of the GCs elicited by EILV-MAYV bound MAYV p62-E1 **(**Fig. 6C-E and S4B**)**. Total and MAYV p62-E1 binding GCs showed classic dark zone and light zone phenotypes **(Fig. S4C)**, and most GC B cells were class-switched **(Fig. S4D-E)**. As Tfh-mediated selection is critical for successful GC responses,[49] we next investigated the Tfh response to EILV-MAYV **(**Fig. 6F **and Fig. S4F)**. Absolute Tfh and GC Tfh counts were significantly increased in mice immunized with EILV-MAYV compared to naïve controls (Fig. 6G). The results collectively demonstrate that immunization with EILV-MAYV induces antigen-specific GC responses.

To further interrogate the humoral response to EILV-MAYV, we evaluated whether plasmablasts (PBs) and plasma cells (PCs) increase in magnitude in EILV-MAYV immunized mice, and whether these antibody-secreting populations produce anti-MAYV antibodies as reflected by binding to MAYV p62-E1 (Fig. 6H-I, **Fig. S4G-H**). EILV-MAYV immunized mice showed a significant increase in absolute numbers of PB/PCs compared to naïve mice (Fig. 6J). Assessment of antigen-specific PB/PCs by intracellular staining revealed that EILV-MAYV primed mice showed detectable numbers of MAYV p62-E1 binding PB/PCs (Fig. 6I, K). While the majority of immunized mice had low numbers of detectable MAYV p62-E1-specific PB/PCs, three mice had more than 500 p62-E1 binding PB/PCs (Fig. 6K). Together with the GC data, these results demonstrate EILV-MAYV's capacity to elicit humoral immune responses.

EILV-MAYV induces durable protection against lethal challenge

The durability of protection induced by EILV-MAYV was assessed by vaccinating 6-to-8-week-old A129 mice subcutaneously with 10^8 PFU and measuring their neutralizing antibody levels every three months for one year after a single dose. We found robust neutralizing antibody responses ($FRNT_{80}$ 1:95 to 1:5376) at 3, 6, 9, and 12 months, with peak titers at six months (Fig. 7A). Upon lethal challenge with MAYV CH (10^4 PFU in the footpad) at one-year post-immunization, the vaccine protected all mice against weight loss and death (Fig. 7B-C), like the protection observed at one-month post-vaccination (Fig. 2). Additionally, vaccinated females appeared to have sterilizing immunity, with no viremia detected, and males had a low but detectable level of viremia(Fig. 7D). We observed no protection from footpad swelling (Fig. 7E), consistent with previous studies (Fig. 2–4), indicating that swelling at the site of infection is refractory to vaccine-induced protection in this model. Overall, these data indicate that EILV-MAYV is durably safe, immunogenic, and efficacious at preventing MAYV disease.

Discussion

MAYV has the potential to emerge in an urban transmission cycle, causing epidemics similar to those of CHIKV.[4,50,51] Its predominance in rural, resource-poor locations in South America necessitates a vaccine

that protects after a single dose. Several anti-MAYV vaccines are in preclinical development. Notably, a virus-like particle vaccine protects mice from lethal challenge after three separate injections.[52] A DNA-based vaccine against MAYV also protects against infection after two doses,[53] and an adenoviral (Adv)-vectored MAYV vaccine protects against MAYV, CHIKV, and Una Virus (UNAV) after two doses.[54,55] However, an efficacious, easy-to-manufacture, refrigerator-stable, single-dose vaccine is still needed.

Here, we describe the generation of an EILV-MAYV vaccine that protects immunocompromised mice from lethal challenge after a single dose and that generates strong humoral and cellular immune responses in immune-intact C57BL/6 mice. Like other EILV chimeras, EILV-MAYV maintains the host range restriction of EILV, yet it is manufacturable in C7/10 cells. Its inability to replicate or cause disease upon intracranial injection of infant CD-1 mice demonstrates its safety even in highly permissive vertebrate animals. These data are consistent with previous studies of EILV-CHIKV, EILV-VEEV, and EILV-EEEV,[21–23] demonstrating that EILV chimeric vaccines are reproducibly replication-incompetent in vertebrates and therefore highly safe vaccine candidates. Our finding that EILV-MAYV is morphologically indistinguishable from MAYV is also consistent with previous studies of other EILV chimeras.[21,23]

Serial passaging of EILV-MAYV resulted in one mutation (E2 G186E) that appeared in two out of three passage replicates. Future studies are needed to assess the impact of the E2 G186E mutation on the antigenicity of the EILV-MAYV vaccine and on its potential to increase titers for more efficient vaccine manufacture in cell culture. However, because no mutations consistently arose in the nonstructural ORF, which is responsible for the failure of EILV chimeras to replicate in vertebrate cells, we conclude that there is little risk of EILV-MAYV developing mutations that result in virulence during the manufacturing process.

Overall, vaccination with a single dose of EILV-MAYV was highly immunogenic and effective at protecting A129 mice from lethal challenge. A single vaccine dose of 10^8 PFU conferred 100% protection up to one-year post-vaccination. The neutralizing antibody response was also durable and remained substantially elevated in A129 mice up to one-year post vaccination. Additionally, vaccination induced durable T cell, B cell, and antibody responses in immunocompetent C57BL/6 mice, indicating that EILV-MAYV is immunogenic in multiple mouse genetic backgrounds. Neutralizing antibody titers of at least 1:20 are a correlate of protection from arthritogenic alphaviruses in humans;[56,57] therefore, the higher neutralizing antibody responses in mice are a promising sign that EILV-MAYV could protect humans from MAYV-induced disease. Additionally, humans typically experience non-lethal MAYV disease, so the ability of EILV-MAYV to protect against lethal murine challenge suggests that EILV-MAYV should protect against musculoskeletal disease in humans. Studies in non-human primates and humans are needed to validate these results.

EILV-MAYV is simple to rapidly manufacture in a laboratory environment, enabling the production of the 10^8 PFU dose that produced the optimal response in these studies. A booster dose of 10^7 PFU of EILV-MAYV resulted in increased neutralizing antibodies and protection from lethal challenge compared to a

single dose of 10^7 PFU. However, this regimen was still inferior to a 10^8 PFU dose, especially in male mice. Even the 10^8 PFU of EILV-MAYV did not cross-protect against disease induced by heterologous arthritogenic alphaviruses, nor did it induce cross-neutralizing antibodies against CHIKV. Interestingly, EILV-MAYV did elicit partial protection against CHIKV viremia, consistent with studies of an Adv-based MAYV vaccine which elicits protection against CHIKV. In the Adv-vectored vaccine system, such cross protection was not reciprocal, as an anti-CHIKV vaccine failed to elicit protection against MAYV.[54,55] Indeed, regimens using an Adv-CHIKV prime dose consistently failed to protect against MAYV, even if an Adv-MAYV booster was used, whereas regimens using an Adv-MAYV prime dose protected against CHIKV regardless of the booster used.[55] This highlights a challenge to the field of alphavirus vaccinology: even closely related alphaviruses can be sufficiently antigenically distinct such that they require separate vaccines, and antigenic difference is not the only factor impacting cross-protection.

The Fc effector functions of anti-MAYV antibodies, and therefore the IgG subclass of those antibodies, play an important role in protection from MAYV in mouse models.[58,59] Specifically, murine IgG1 was inferior to murine IgG2A in controlling MAYV infection.[58,59] It is therefore essential to closely examine the type of immune response induced by MAYV vaccine candidates. EILV-MAYV elicits a focused germinal center B cell response, with the majority of GC B cells class-switching to non-IgG1 isotypes. Animals vaccinated with EILV-MAYV produced both germinal center B cells and PB/PC capable of binding MAYV P62-E1, which is consistent with the rapid induction of neutralizing antibody and steady increase in neutralizing antibody observed for several months following vaccination. Further studies are needed to understand more specifically the isotypes of the antibodies elicited by EILV-MAYV, along with the Th1/Th2 ratio of the strong T cell response.

Although EILV-MAYV acts as a non-replicating vaccine in mammals, similar to an inactivated or virus-like particle vaccine, a single dose of EILV-MAYV induces long-lasting immunity. In contrast, inactivated vaccines typically induce immunity that decays rapidly.[60] We hypothesize that EILV-MAYV stimulates a stronger innate immune response than other non-replicating vaccines because it carries viral genomic RNA that enters the host cell and may act as a pathogen-associated molecular pattern, binding to single-stranded RNA sensing proteins and activating the cell's innate immune response[21]. This RNA may also be translated into the nonstructural polyprotein, which could contribute to the immune response.[26] Unlike VLPs, which require simultaneous transfection of cells with multiple viral genes, the production of EILV-MAYV simply requires passaging the virus in cell culture. EILV-MAYV is therefore an immunogenic and easy-to-produce vaccine candidate

At lower vaccine doses, we observed sex based differences in protection elicited by EILV-MAYV, with female mice generating stronger immune responses and being more robustly protected from challenge than male mice. This differential phenotype is consistent with observations in humans and animal models that females tend to mount stronger antiviral immune responses, and males tend to exhibit more severe disease from a variety of viral infections.[61] Sex hormones, such as estrogen, testosterone, and P4, have strong positive and negative impacts on the magnitude of immune responses, depending on

the concentration of the hormone and the level of expression of hormone receptors.[62] For example, estrogen response elements in the NF-κB and TNF signaling pathways mediate increased antibody responses to the influenza vaccine in females.[63] However, further studies are needed to examine how individual sex hormones may impact specific immune-cell types in the context of EILV-MAYV vaccination. Regardless of our observations of sex-based differences, providing a higher vaccine dose or a booster dose resolved these differences.

These studies provide evidence of the safety and efficacy of EILV-MAYV in a small animal model. However, mice are limited in their ability to model vaccine-induced protection from MAYV disease in humans. The short lifespan of mice precludes studies of immunogenicity for longer than one year. In these studies, an unpurified research-grade vaccine was used. Further testing will be needed in higher vertebrates using GMP-grade vaccine batches as this platform is developed. Additionally, appropriate vaccine doses for use in humans may not be extrapolated from effective doses in mice, and could be clarified in such follow-up studies.

In conclusion, EILV-MAYV is a safe and effective vaccine in mouse models. Its immunogenicity, safety profile, and ease of production make it a promising vaccine candidate for further advancement through pre-clinical trials. Future studies in large-animal models, including non-human primates, are needed to identify ideal vaccine formulations for use in human clinical trials.

Declarations

Author contributions:

Jennifer Diaz produced the relevant vaccine and virus stocks and executed all animal studies involving lethal challenge and all studies involving infant mice, along with associated assays. Nisha Tapryal and Scott C. Weaver contributed to A129 and CD-1 mouse studies, vaccine production, and associated assays. Ellie Hajovsky, Jessica Plante, Amanda Mareth, Chanida Fongsaran, and Rachel Colwell also assisted with these studies. Mauricio V. Padilla, Kristy M. Waldrep, Kristyn Gonzales, performed the B-cell studies described in **Fig. 6**, with guidance from Robert K. Abbott. Xueyong Xu, with guidance from Richard J. Kuhn, performed cryo-electron microscopy and associated analysis (Fig. 1, **S1**). Jesse Erasmus, Farooq Nasar, and Scott C. Weaver conceptualized the EILV-MAYV vaccine, and Dr. Erasmus created the EILV-MAYV infectious clone. Awadalkareem Adam and Andrei Siniavin, with guidance from Tian Wang, performed the immunogenicity studies described in **Fig. 5** and **Figure S3A-B**. Shilpa Sanapala, with guidance from Michael S. Diamond, performed the fluorescence-based neutralization assays described in **Figure S3C-D**. Haiping Hao performed RNA sequencing and associated analysis (**Figure S2**). Michael S. Diamond, Richard J. Kuhn, Tian Wang, Kenneth S. Plante, and Robert K. Abbott supervised and advised on substantial aspects of this project. Scott C. Weaver supervised and advised on the conceptualization and execution of all aspects of this project.

Acknowledgements

We thank the World Reference Center for Emerging Viruses and Arboviruses for anti-MAYV antibodies used in immunostaining, Dr. Chris Nelson and Dr. Daved Fremont for generously providing the p62-E1 flow cytometry probes, and Dr. Lauren Williamson for providing anti-MAYV mAbs. Guadalupe Oliva Escudero assisted with some of the neutralizing antibody assays

Data availability:

All data described in this manuscript are available in ImmPort.

References

1. Wei LLL, Tom R, Kim YC (2024) Mayaro Virus: An Emerging Alphavirus in the Americas. Viruses 16:1297
2. Campos M et al (2025) Genetics of range expansion and admixture of Aedes aegypti populations in California. BMC Genomics 26:1135
3. Abbasi E (2026) Global epidemiology and evolutionary dynamics of arboviruses: A systematic review of surveillance, control strategies, and emerging threats. Dialogues Health 8:100280
4. Mackay IM, Arden KE (2016) Mayaro virus: a forest virus primed for a trip to the city? Microbes Infect 18:724–734
5. Tesh RB et al (1999) Mayaro Virus Disease: An Emerging Mosquito-Borne Zoonosis in Tropical South America. Clin Infect Dis 28:67–73
6. Diagne CT et al (2020) Mayaro Virus Pathogenesis and Transmission Mechanisms. Pathogens 9:738
7. Santiago FW et al (2015) Long-Term Arthralgia after Mayaro Virus Infection Correlates with Sustained Pro-inflammatory Cytokine Response. PLoS Negl Trop Dis 9:e0004104
8. Halsey ES et al (2013) Mayaro Virus Infection, Amazon Basin Region, Peru, 2010–2013. Emerg Infect Dis 19:1839–1842
9. Robinson MC (1955) An epidemic of virus disease in Southern Province, Tanganyika territory, in 1952–1953. I. Clinical Features. Trans R Soc Trop Med Hyg 49:28–32
10. Weaver SC, Chen R, Diallo M (2020) Chikungunya Virus: Role of Vectors in Emergence from Enzootic Cycles. Ann Rev Entomol 65:313–332
11. Weaver SC, Forrester NL, Chikungunya (2015) Evolutionary history and recent epidemic spread. Antiviral Res 120:32–39
12. Wan S et al (2025) Viral Load Dynamics of Chikungunya Virus in Human Specimens — Foshan City, Guangdong Province, China, 2025. China CDC Wkly 7:1067–1072

13. Sagar R et al (2024) Viremia and clinical manifestations in acute febrile patients of Chikungunya infection during the 2016 CHIKV outbreak in Delhi, India. Infect Med 3:100088
14. Appassakij H, Khuntikij P, Kemapunmanus M, Wutthanarungsan R, Silpapojakul K (2013) Viremic profiles in asymptomatic and symptomatic chikungunya fever: a blood transfusion threat? Transfusion 53:2567–2574
15. Severini F et al (2018) Vector competence of Italian Aedes albopictus populations for the chikungunya virus (E1-226V). PLoS Negl Trop Dis 12:e0006435
16. Agha SB et al (2017) Vector competence of populations of Aedes aegypti from three distinct cities in Kenya for chikungunya virus. PLoS Negl Trop Dis 11:e0005860
17. Beranek MD, Giayetto O, Fischer S, Diaz A (2024) Assessment of Mayaro virus vector competence of the mosquito Aedes aegypti (Linnaeus, 1762) populations in Argentine using dose-response assays. Med Vet Entomol 38:234–243
18. Long KC et al (2011) Experimental Transmission of Mayaro Virus by Aedes aegypti. https://doi.org/10.4269/ajtmh.2011.11-0359 doi:10.4269/ajtmh.2011.11-0359
19. Tsetsarkin KA et al (2009) Epistatic Roles of E2 Glycoprotein Mutations in Adaption of Chikungunya Virus to Aedes Albopictus and Ae. Aegypti Mosquitoes. PLoS ONE 4:e6835
20. Silva-Ramos CR, Mejorano-Fonseca JA, Hidalgo M, Rodríguez-Morales AJ, Faccini-Martínez ÁA, Clinical (2023) Epidemiological, and Laboratory Features of Mayaro Virus Infection: a Systematic Review. Curr Trop Med Rep 10:309–319
21. Erasmus JH et al (2017) A chikungunya fever vaccine utilizing an insect-specific virus platform. Nat Med 23:192–199
22. Adam A et al (2024) A safe insect-based chikungunya fever vaccine affords rapid and durable protection in cynomolgus macaques. npj Vaccines 9:1–14
23. Erasmus JH et al (2018) Novel Insect-Specific Eilat Virus-Based Chimeric Vaccine Candidates Provide Durable, Mono- and Multivalent, Single-Dose Protection against Lethal Alphavirus Challenge. J Virol 92. 10.1128/jvi.01274-17
24. Adam A et al (2021) Optimized production and immunogenicity of an insect virus-based chikungunya virus candidate vaccine in cell culture and animal models. Emerging Microbes Infections 10:305–316
25. Nasar F et al (2012) Eilat virus, a unique alphavirus with host range restricted to insects by RNA replication. *Proceedings of the National Academy of Sciences* 109, 14622–14627
26. Nasar F, Gorchakov RV, Tesh RB, Weaver SC (2014) Eilat Virus Host Range Restriction Is Present at Multiple Levels of the Virus Life Cycle. J Virol 89:1404–1418
27. Meshram CD et al (2018) Multiple Host Factors Interact with the Hypervariable Domain of Chikungunya Virus nsP3 and Determine Viral Replication in Cell-Specific Mode. J Virol 92. 10.1128/jvi.00838 - 18

28. Webb EM et al (2019) Effects of Chikungunya virus immunity on Mayaro virus disease and epidemic potential. Sci Rep 9:20399
29. Weise WJ et al (2014) A Novel Live-Attenuated Vaccine Candidate for Mayaro Fever. PLoS Negl Trop Dis 8:e2969
30. Erasmus JH et al (2015) Utilization of an Eilat Virus-Based Chimera for Serological Detection of Chikungunya Infection. PLoS Negl Trop Dis 9:e0004119
31. Mukherjee S et al (2016) Enhancing dengue virus maturation using a stable furin over-expressing cell line. Virology 497:33–40
32. Kim AS et al (2021) Pan-protective anti-alphavirus human antibodies target a conserved E1 protein epitope. Cell 184:4414–4429e19
33. Campos RK et al (2020) Adenoviral-Vectored Mayaro and Chikungunya Virus Vaccine Candidates Afford Partial Cross-Protection From Lethal Challenge in A129 Mouse Model. Front Immunol 11
34. Ribeiro-Filho HV et al (2021) Cryo-EM structure of the mature and infective Mayaro virus at 4.4 Å resolution reveals features of arthritogenic alphaviruses. Nat Commun 12:3038
35. Beier S, Bolger AM, Bolger ME, Schwacke R, Usadel B (2026) Trimmomatic: a decade of feature-rich, high-performance NGS read preprocessing. Bioinformatics 42:btag331
36. Earnest JT et al (2019) Neutralizing antibodies against Mayaro virus require Fc effector functions for protective activity. J Exp Med 216:2282–2301
37. Han X et al (2025) Neutralizing antibodies against Chikungunya virus and structural elucidation of their mechanism of action. Nat Commun 16:9682
38. Pal P et al (2013) Development of a highly protective combination monoclonal antibody therapy against Chikungunya virus. PLoS Pathog 9:e1003312
39. Bankhead P et al (2017) QuPath: Open source software for digital pathology image analysis. Sci Rep 7:16878
40. Malonis RJ et al (2021) Near-germline human monoclonal antibodies neutralize and protect against multiple arthritogenic alphaviruses. *Proceedings of the National Academy of Sciences* 118, e2100104118
41. Chmielewski D et al (2021) Near-atomic resolution Cryo-EM structure of Mayaro virus identifies key structural determinants of alphavirus particle formation. 01.14.425226 Preprint at https://doi.org/10.1101/2021.01.14.425226(2021)
42. Ribeiro-Filho HV et al (2021) Cryo-EM structure of the mature and infective Mayaro virus at 4.4 Å resolution reveals features of arthritogenic alphaviruses. Nat Commun 12:3038
43. Hasan SS et al (2018) Cryo-EM Structures of Eastern Equine Encephalitis Virus Reveal Mechanisms of Virus Disassembly and Antibody Neutralization. Cell Rep 25:3136–3147e5
44. Research C, for BE (2025) and. Characterization and Qualification of Cell Substrates and Other Biological Materials Used in the Production of Viral Vaccines for Infectious Disease Indications.

https://www.fda.gov/regulatory-information/search-fda-guidance-documents/characterization-and-qualification-cell-substrates-and-other-biological-materials-used-production

45. Anderson EJ, Knight AC, Heise MT, Baxter VK (2023) Effect of Viral Strain and Host Age on Clinical Disease and Viral Replication in Immunocompetent Mouse Models of Chikungunya Encephalomyelitis. Viruses 15:1057
46. Ryman KD et al (2007) Early restriction of alphavirus replication and dissemination contributes to age-dependent attenuation of systemic hyperinflammatory disease. J Gen Virol 88:518–529
47. Victora GD, Nussenzweig MC (2022) Germinal Centers. Annu Rev Immunol 40:413–442
48. Eisen HN (2014) Affinity Enhancement of Antibodies: How Low-Affinity Antibodies Produced Early in Immune Responses Are Followed by High-Affinity Antibodies Later and in Memory B-Cell Responses. Cancer Immunol Res 2:381–392
49. Crotty ST, Follicular Helper (2019) Cell Biology: A Decade of Discovery and Diseases. Immunity 50:1132–1148
50. Beranek MD, Giayetto O, Fischer S, Diaz A (2024) Assessment of Mayaro virus vector competence of the mosquito Aedes aegypti (Linnaeus, 1762) populations in Argentine using dose-response assays. Med Vet Entomol 38:234–243
51. Smith GC, Francy DB (1991) Laboratory studies of a Brazilian strain of Aedes albopictus as a potential vector of Mayaro and Oropouche viruses. J Am Mosq Control Assoc 7:89–93
52. Kim YC et al (2024) Immunogenic recombinant Mayaro virus-like particles present natively assembled glycoprotein. npj Vaccines 9:243
53. Choi H et al (2019) Protective immunity by an engineered DNA vaccine for Mayaro virus. PLoS Negl Trop Dis 13:e0007042
54. Campos RK et al (2020) Adenoviral-Vectored Mayaro and Chikungunya Virus Vaccine Candidates Afford Partial Cross-Protection From Lethal Challenge in A129 Mouse Model. Front Immunol 11
55. Weber WC et al (2024) Nonreciprocity in CHIKV and MAYV Vaccine-Elicited Protection. Vaccines 12:970
56. Milligan GN, Schnierle BS, McAuley AJ, Beasley D (2019) W. C. Defining a correlate of protection for chikungunya virus vaccines. Vaccine 37:7427–7436
57. Yoon I-K et al (2015) High Rate of Subclinical Chikungunya Virus Infection and Association of Neutralizing Antibody with Protection in a Prospective Cohort in The Philippines. PLoS Negl Trop Dis 9:e0003764
58. Earnest JT et al (2019) Neutralizing antibodies against Mayaro virus require Fc effector functions for protective activity. J Exp Med 216:2282–2301
59. Earnest JT et al (2021) The mechanistic basis of protection by non-neutralizing anti-alphavirus antibodies. Cell Rep 35:108962
60. Andey T, Soni S, Modi S (2024) Chapter 3 - Conventional vaccination methods: Inactivated and live attenuated vaccines. in *Advanced Vaccination Technologies for Infectious and Chronic Diseases*(eds

Chavda, V. P., Vora, L. K. & Apostolopoulos, V.) 37–50Academic Press. 10.1016/B978-0-443-18564-9.00030-8

61. Takahashi T, Iwasaki A (2021) Sex differences in immune responses. Science 371:347–348
62. Dunn SE, Perry WA, Klein SL (2024) Mechanisms and consequences of sex differences in immune responses. Nat Rev Nephrol 20:37–55
63. Park H-S et al (2026) Sex and age differences in antibody responses to seasonal influenza vaccination are mediated by estrogenic upregulation of NF-κB and TNF signaling in B cells. mBio 17:e01435–e01426

Figures

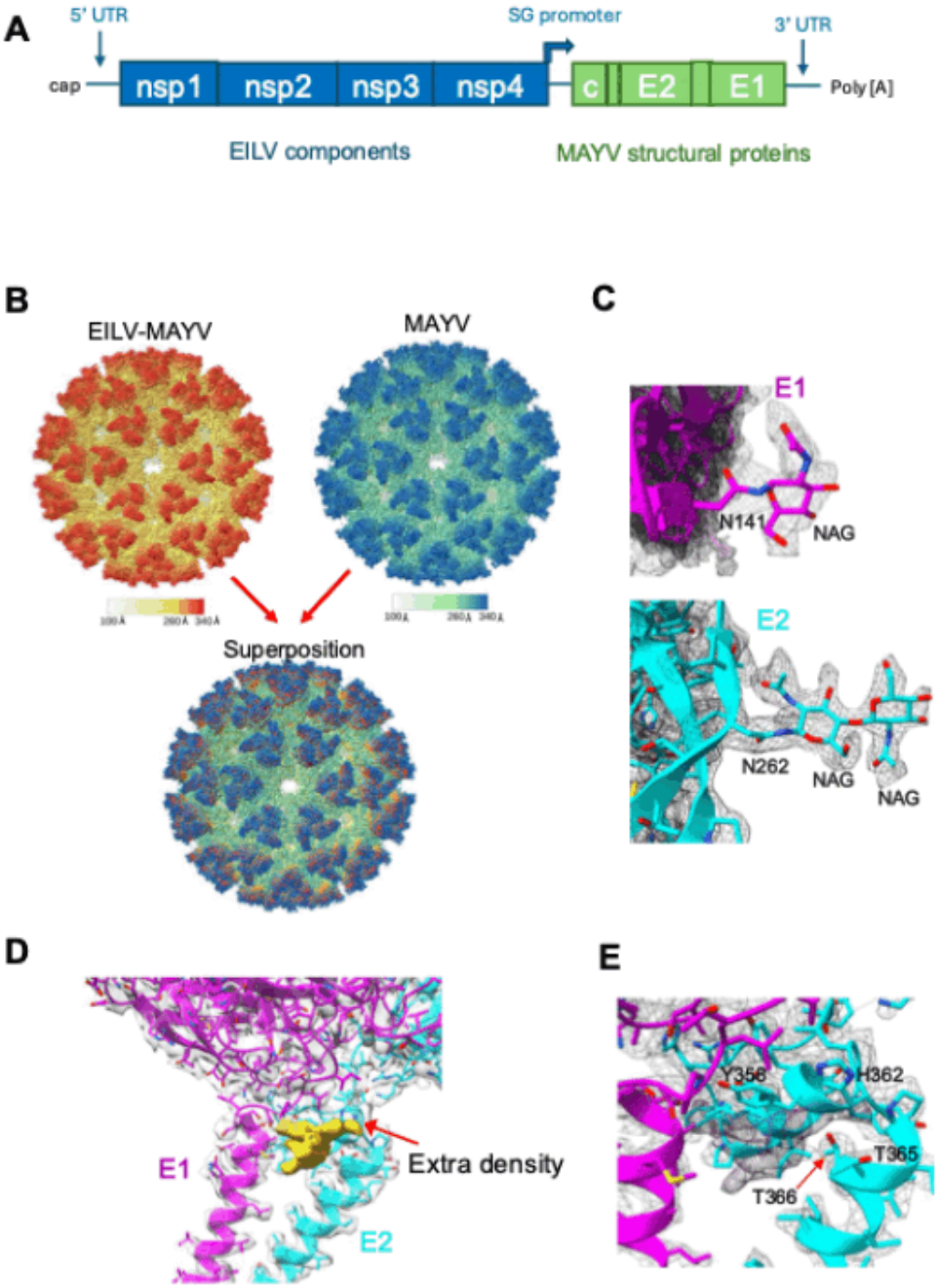


Figure 1

Cryo-EM structure of EILV-MAYV. (**A**) Diagram of the EILV-MAYV genome. (**B**) Comparison of the cryo-EM structures of EILV-MAYV and MAYV. The molecular surfaces are colored radially. (**C**) N-glycosylation sites observed in the E1–E2 ectodomain of the EILV-MAYV cryo-EM structure. (**D**) Extra density observed within the cavity between E1 and E2 at the outer leaflet of the membrane. (**E**) Close-up view of the extra density and the surrounding residues.

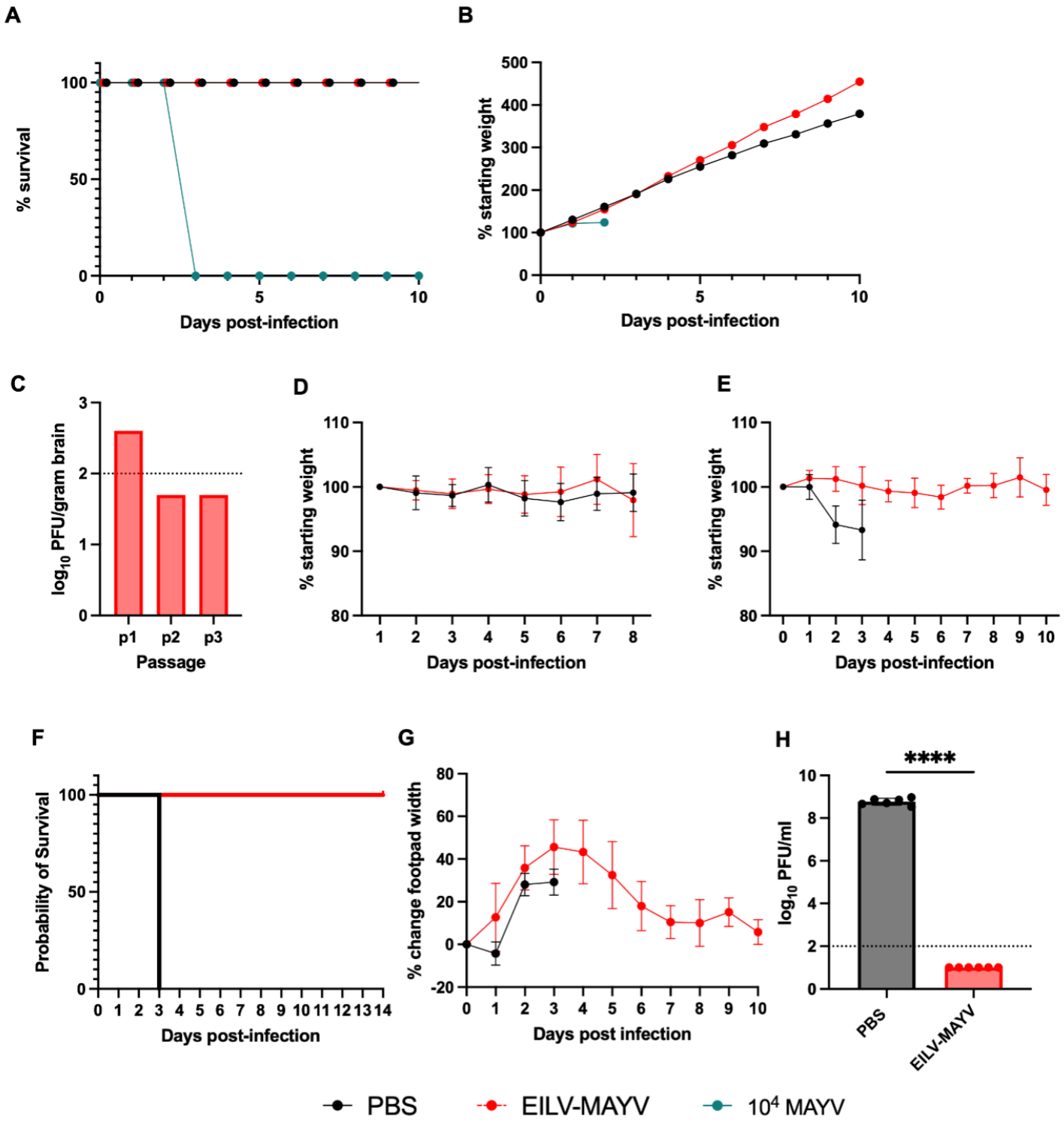


Figure 2

EILV-MAYV is safe and protects against MAYV challenge. (**A, B**) One-to-three-day-old CD-1 mice were intracranially inoculated with PBS, EILV-MAYV, or MAYV, and their weight and health were monitored daily. Mice were euthanized at the onset of symptoms or upon failure to gain weight (n = 1 litter, one experiment) (**C**) One litter each of eight to ten one-to-three-day-old CD-1 mice were intracranially inoculated with 10^8 PFU of EILV-MAYV, and after two days their brains were harvested and homogenized in PBS (10% w/v brain/PBS). Brain homogenate was subsequently inoculated into the brains of

additional CD-1 mice for two additional passages, and homogenate was titered by plaque assay after each passage (n = 1 litter, one experiment). (**D-H**) Male and female six-to-eight-week-old A129 mice were vaccinated s.c. with 10^8 PFU of EILV-MAYV and weighed daily for one week (**D**). At 28 days post-vaccination, animals were challenged subcutaneously in the footpad with 10^4 PFU of MAYV. Weight (**E**), survival (**F**), and footpad swelling (**G**) were assessed daily (n = 6 mice, one experiment). (**H**) Viremia was measured by plaque assay at two-days post-infection LOD, 2 $\log_{10}$ PFU/ml. Statistical analysis: (**D, E, G**) Graphs show mean and standard deviation. (**H**) student's t test. ****, p < .0001.

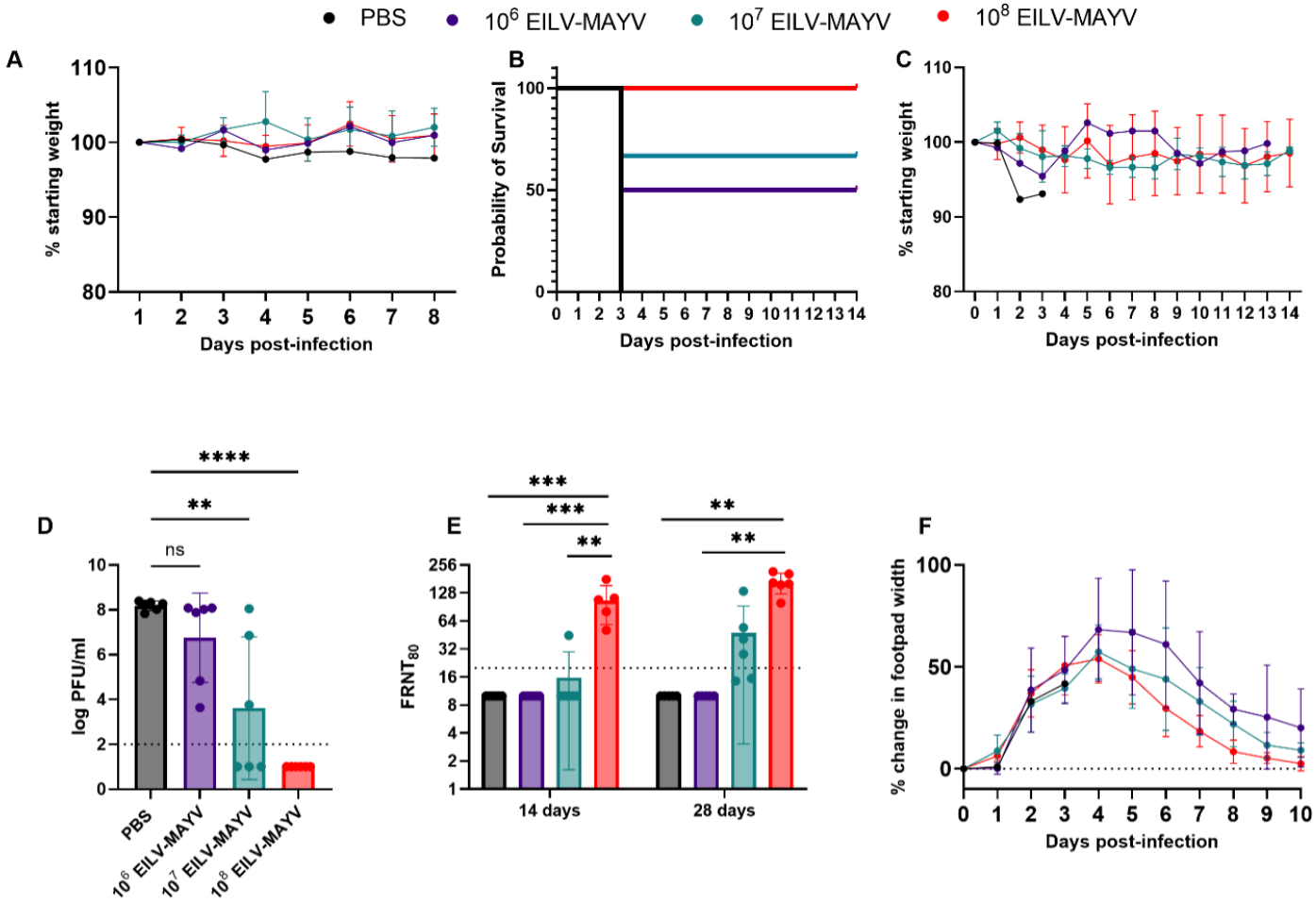


Figure 3

EILV-MAYV dose-dependently protects against MAYV challenge. Six-to-eight-week-old male and female A129 mice were vaccinated s.c. with the indicated dose of EILV-MAYV or sham-vaccinated with PBS and weighed daily for one week (**A**). At 28 days post-vaccination, animals were challenged subcutaneously in the footpad with 10^4 PFU of MAYV. Survival (**B**), and weight (**C**) were assessed daily (n = 6 mice, one experiment). (**D**) Viremia was measured by plaque assay at two-days post-infection (LOD, 2 $\log_{10}$ PFU/ml). (**E**) Serum was harvested at 14 and 28 days post-vaccination, and neutralizing antibodies were assessed by FRNT (LOD, 1/20). (**F**) Footpad swelling was assessed daily. Statistical analysis: (**A, C-F**)

Graphs show mean values and standard deviation. (**D**) two-way ANOVA with Tukey's post-test. (**E**) Kruskal-Wallis test with Dunn's post-test. *, p < 0.05; **, p < 0.01; ***, p < 0.001****, p < 0.0001.

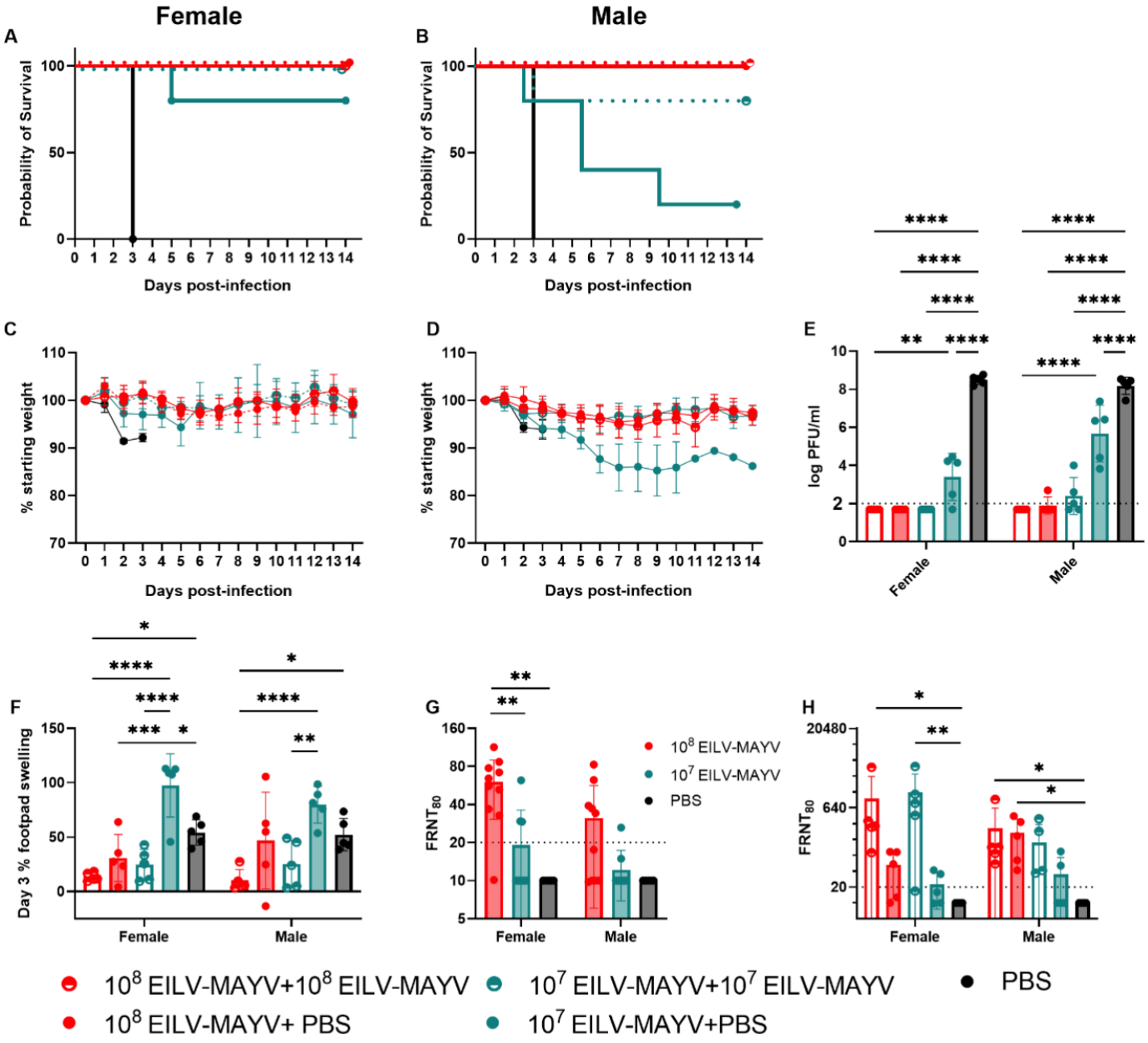


Figure 4

Booster doses improve protection by EILV-MAYV. Six-to-eight-week-old male and female A129 mice were vaccinated s.c. with the indicated dose of EILV-MAYV or sham-vaccinated with PBS (n=5 mice, one experiment). At 28 days post-prime, animals were administered a booster dose of vaccine or PBS. At 28 days post-boost, animals were challenged subcutaneously in the footpad with 10^4 PFU of MAYV. Survival (females **A**, males **B**), and weight (females **C**, males **D**) were assessed daily. (**E**) Viremia was measured by plaque assay at two-days post-infection (LOD, 2 $\log_{10}$ PFU/ml). (**F**) Day three footpad swelling. (**G, H**)

Serum was harvested at the time of booster administration and at the time of challenge, and neutralizing antibodies were assessed by FRNT (LOD, 1/20). Statistical analysis: (**C-H**) Graphs show mean values and standard deviations. (**F**) two-way ANOVA with Tukey's post-test.(**G, H**) Kruskal-Wallis test with Dunn's post-test. *, p < 0.05; **, p < 0.01; ***, p < 0.001****, p < 0.0001.

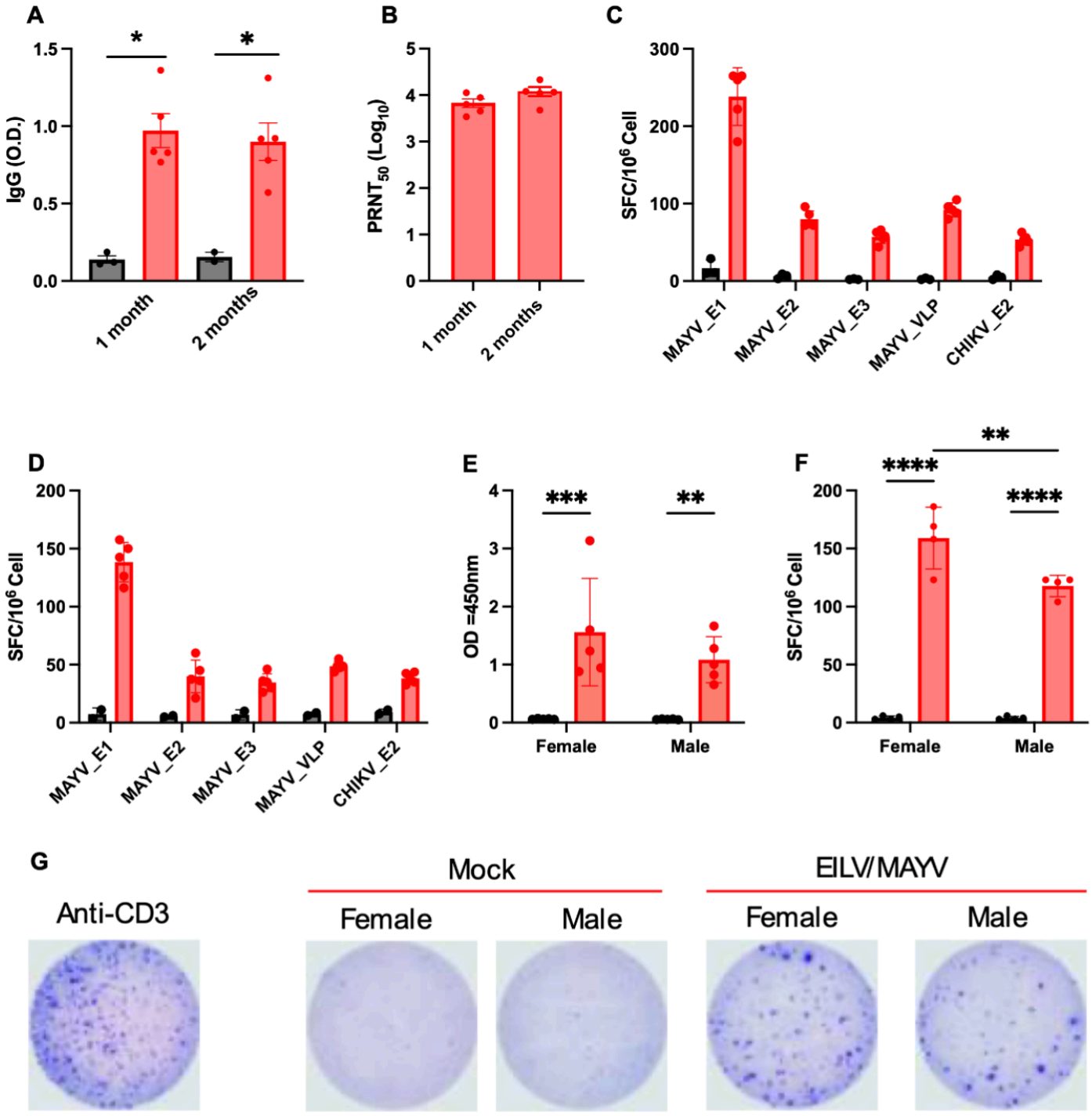


Figure 5

EILV-MAYV elicits T cell responses. (**A-B**) Serum was harvested at one-month or two-months post-vaccination from female C57BL/6J mice vaccinated i.p. with 10^8 PFU of EILV-MAYV (n=5) or PBS (n=3) (one experiment). (**C-D**) Splenocytes were harvested at one-month (**C**) or two-months (**D**) post-

vaccination from C57BL/6J mice vaccinated i.p. with 10^8 PFU of EILV-MAYV or PBS (n=5 per group, one experiment). (**E-F**) Serum and splenocytes were harvested at one-month or two-months post-vaccination from male and female C57BL/6J mice vaccinated i.p. with 10^8 PFU of EILV-MAYV (n=5) or PBS (n=3 at one-month, n=2 at two-months) (one experiment). (**A, E**) ELISA-based measurements of antibody binding to MAYV E2 protein. (**B**) Anti-MAYV neutralizing antibodies were measured by PRNT assay. (**C, D, F, G**) T cells were restimulated with the indicated antigen, and ELISPOT assay was performed. Counts of E1-specific T cells/10^6 splenocytes were compared. (**G**) Representative images of ELISPot assay wells. Statistical analysis: (**A, C-F**) two-way ANOVA followed by Tukey's post-test. (**B**) student's t-test. *, $p < 0.05$; **, $p < 0.01$; ***, $p < 0.001$****, $p < 0.0001$. (**A-F**) Means and standard deviations are shown.

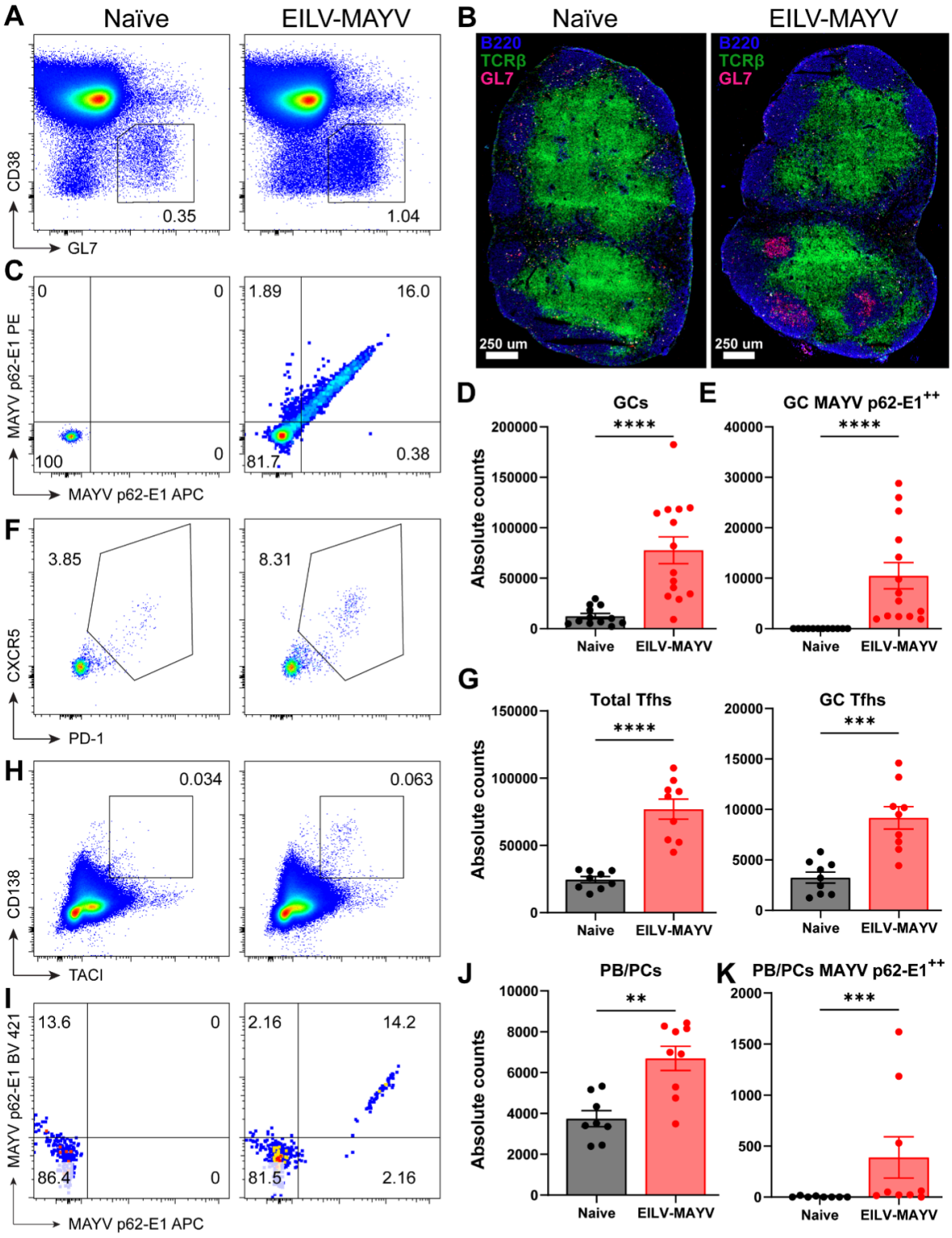


Figure 6

C57BL/6J mice were vaccinated s.c. with 10^7 PFU of EILV-MAYV (**A**) Representative flow cytometry plots from immunized and naïve mice show frequencies of germinal center B cells (GCs) collected from inguinal lymph nodes (iLNs) harvested 12 days post-immunization. Plots are pre-gated on scatter/singlet/live/$B220^+/CD4^-$. (**B**) Representative histology of germinal centers induced in immunized mice at day 12 after vaccination with 10^7 PFU of EILV-MAYV. Blue B220, B cells; green TCRβ, T cells; and

red GL7, GCs. (**C**) Representative flow cytometry plots from immunized and naïve mice show frequencies of MAYV p62-E1-binding (Ag^+) GC B cells collected from inguinal lymph nodes (iLNs) harvested 12 days post-immunization. (**D**) Absolute counts of GCs in harvested iLNs, gated as in A. (**E**) Absolute counts of MAYV p62-$E1^-$binding GC B cells in harvested iLNs, gated as in C. (**F**) Representative flow cytometry plots from immunized and naïve mice show frequencies of GC T follicular helper (Tfh) cells collected from iLNs harvested 12 days post-immunization. Plots are pre-gated on scatter/singlet/live/$B220^-$/$CD4^+$/$CD90.2^{lo/-}$/$FoxP3^-$/$CXCR5^{hi}$/$PD\text{-}1^{hi}$. (**G**) Bar graphs display the absolute counts in harvested iLNs of both the total Tfh population, gated on scatter/singlet/live/$B220^-$/$CD4^+$/$FoxP3^-$/$CXCR5^{hi}$/$PD\text{-}1^{hi}$, and the absolute counts of the GC Tfh population, gated as in F. (**H-K**) Representative flow cytometry plots (**H-I**) and summary counts (**J-K**) from immunized and naïve mice show frequencies of plasmablasts/plasma cells (PB/PCs) (**H, J**) and MAYV p62-E1 binding PB/PCs (**I, K**) collected from iLNs harvested 12 days post-immunization. **(A, C-E)** n=3-9, 2 experiments. **(F-K)** n=9, 1 experiment. **(D-E, G, J-K)** Statistical analysis: Mann-Whitney U test. ** = $p < 0.01$, *** = $p < 0.001$, **** = $p < 0.0001$.

EILV-MAYV elicits germinal center B cell responses

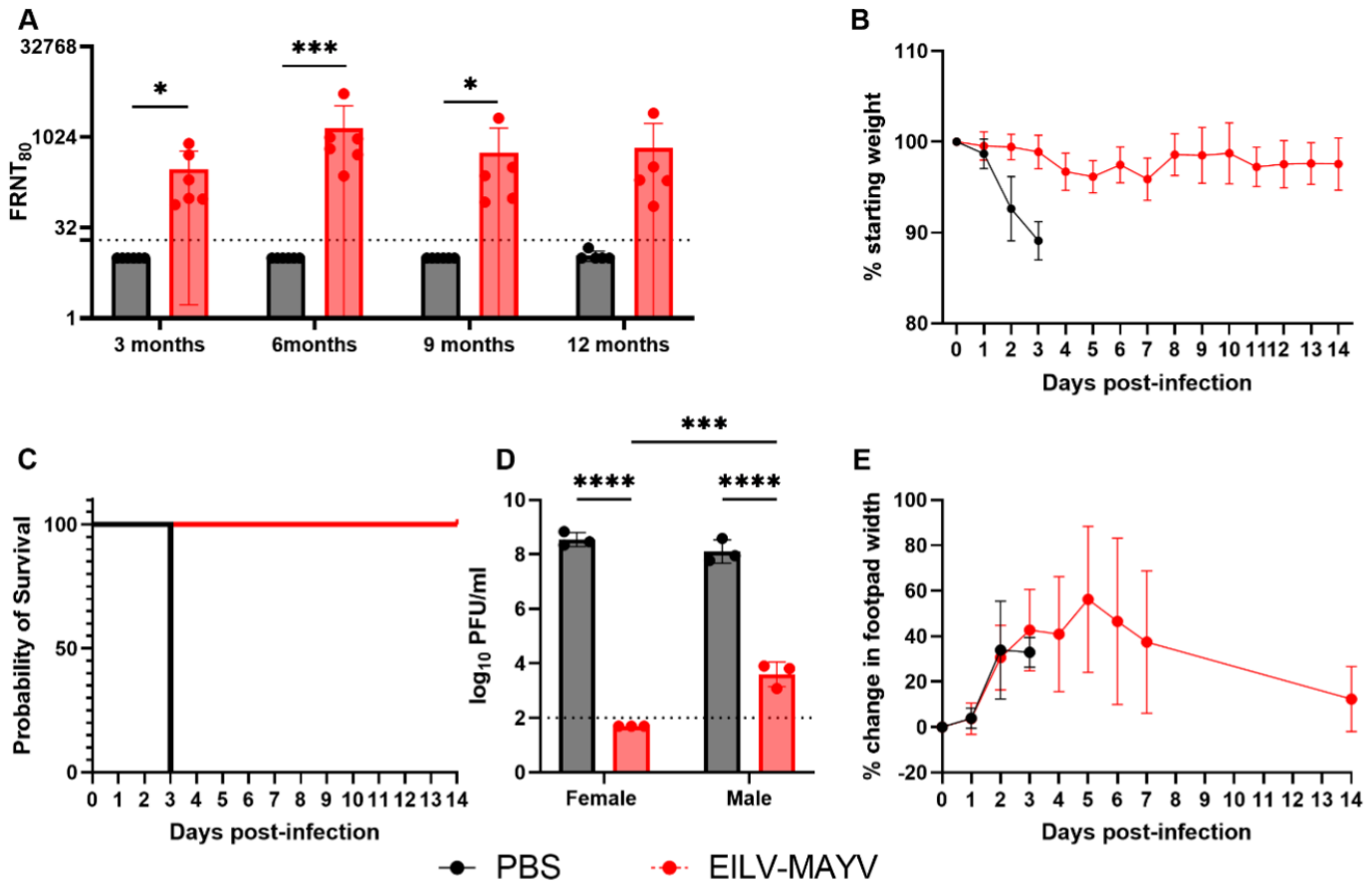


Figure 7

EILV-MAYV induces durable protection against MAYV. Male and female six-to-eight-week-old A129 mice were vaccinated s.c. with 10^8 PFU of EILV-MAYV and weighed daily for one week (n =6 mice, one experiment). At one-year post-vaccination, animals were challenged subcutaneously in the footpad with 10^4 PFU of MAYV. (**A**) Serum was harvested at time 1, 3, 6, 9, and 12 months post-vaccination, and neutralizing antibodies were assessed by FRNTs (LOD = 1:20). (**B, C, E**) Weights, survival, and footpad swelling were assessed daily. (**A, B, D, E**) Graphs show mean values and standard deviations. (**D**) Viremia was measured by plaque assay at 2 days post-infection (LOD= 2 $\log_{10}$ PFU/ml). Statistical analysis: (**A**) Kruskal-Wallis test with Dunn's post-test. (**D**) two-way ANOVA with Tukey's post-test. *, p < .05; **, p < .01; ***, p < .001****, p < .0001.

Supplementary Files

This is a list of supplementary files associated with this preprint. Click to download.

- TableS2sequencing.pdf
- TableS1cryoEM.pdf